Origin of orthorhombic transition, magnetic transition, and shear-modulus softening in iron pnictide superconductors: Analysis based on the orbital fluctuations theory

Hiroshi Kontani,[1] Tetsuro Saito,[1] and Seiichiro Onari[2]
[1]*Department of Physics, Nagoya University and JST, TRIP, Furo-cho, Nagoya 464-8602, Japan*
[2]*Department of Applied Physics, Nagoya University and JST, TRIP, Furo-cho, Nagoya 464-8602, Japan*
(Received 22 March 2011; published 25 July 2011)

The main features in iron pnictide superconductors are summarized as (i) the orthorhombic transition accompanied by a remarkable softening of the shear modulus, (ii) high-T_c superconductivity close to the orthorhombic phase, and (iii) stripe-type magnetic order induced by orthorhombicity. To present a unified explanation for these features, we analyze the multi-orbital Hubbard-Holstein model with Fe-ion optical phonons based on the orbital fluctuation theory. In the random-phase approximation (RPA), a small electron-phonon coupling constant ($\lambda \sim 0.2$) is enough to produce large orbital (charge quadrupole) fluctuations. The most divergent susceptibility is the O_{xz}-antiferroquadrupole (AFQ) susceptibility, which causes s-wave superconductivity without sign reversal (s_{++}-wave state). At the same time, divergent development of $O_{x^2-y^2}$-ferroquadrupole (FQ) susceptibility is brought about by the "two-orbiton process" with respect to the AFQ fluctuations, which is absent in the RPA. The derived FQ fluctuations cause the softening of the C_{66} shear modulus, and its long-range order not only triggers the orthorhombic structure transition, but also induces the instability of the stripe-type antiferromagnetic state. In other words, the condensation of composite bosons made of two orbitons gives rise to the FQ order and structure transition. Therefore, the theoretically predicted multi-orbital criticality presents a unified explanation for the above-mentioned features of iron pnictide superconductors.

DOI: 10.1103/PhysRevB.84.024528 PACS number(s): 74.70.Xa, 74.20.Rp, 74.25.Kc

I. INTRODUCTION

In iron pnictide superconductors,[1] both spin and orbital degrees of freedom play important roles on various electronic properties, such as high-T_c superconductivity, orthorhombic structure transition, and magnetic transition. As for the origin of the superconductivity, a fully gapped sign-reversing s-wave ($s_{\pm}$-wave) state had been studied based on spin fluctuation theories.[2–5] The origin of the spin fluctuations is the intra-orbital nesting and the Coulomb interaction. However, the robustness of T_c against the randomness in iron pnictides indicates the absence of sign reversal in the superconducting (SC) gap.[6–8]

Later, an orbital-fluctuation-mediated s-wave state without sign reversal (s_{++}-wave) was proposed based on the Hubbard-Holstein (HH) model.[9–11] The origin of the orbital fluctuations is the interorbital nesting and the electron-phonon (e-ph) interactions due to non-A_{1g} optical phonons. One of the merits of this scenario is the robustness of the s_{++}-wave state against impurities. Another merit is that the close relation between T_c and the crystal structure revealed by Lee,[12] namely that T_c becomes the highest when the As_4 cluster is a regular tetrahedron, is automatically explained.[10] Moreover, the orbital-fluctuation-mediated s_{++}-wave state scenario is consistent with the large SC gap on the z^2-orbital band in Ba122 systems,[10] observed by bulk-sensitive laser angle-resolved photoemission spectroscopy (ARPES) measurement.[13]

The "resonance-like" hump structure in the neutron inelastic scattering[14] is frequently explained as the spin resonance due to the sign reversal in the SC gap.[15,16] However, an experimental hump structure is well reproduced in terms of the s_{++}-wave SC state, rather than the $s_{\pm}$-wave SC state, by taking the suppression in the inelastic scattering $\gamma(\omega)$ for $|\omega| \leqslant 3\Delta$ in the SC state (dissipation mechanism).[17,18] To distinguish between both SC states, measurements of a phonon spectral function for $|\omega| \lesssim 2\Delta$ would be useful.[19] In the normal state, prominent non-Fermi-liquid transport phenomena in ρ and R_H (Ref. 20) are frequently ascribed to the evidence of spin fluctuations.[21] However, they are also explained by the development of antiferro-orbital fluctuations.[11]

To identify the mechanism of superconductivity, we have to understand the origin of the ordered state, although it is still unsolved in iron pnictides. For example, in many heavy fermion superconductors, the SC phase appears next to the spin-density-wave (SDW) state, indicating the occurrence of spin-fluctuation-mediated superconductivity. In contrast, the ordered state in iron pnictides is not a simple SDW state: In fact, the tetragonal to orthorhombic structure transition occurs at $T_S \sim 100$ K, usually above the SDW transition temperature T_N.[22] In addition, a large imbalance of xz and yz orbitals at the Fermi level and reconstruction of the Fermi surfaces (FS's) had been observed by ARPES measurements.[23–25] These results indicate that the ferro orbital-density wave (ODW) is the origin of the orthorhombic structure transition. The SDW state may originate from the in-plane anisotropy in the exchange interaction ($J_{1a} \neq J_{1b}$) associated with the ODW order.[26]

In addition, prominent symmetry breaking $C_4 \to C_2$ is realized in detwinned 122 systems even above T_S and T_N, under very small uniaxial pressure. For example, it is recognized as the large in-plane anisotropy in the resistivity[27,28] and the optical conductivity[29] at $T^* \sim 200$ K, which is much higher than T_S and T_N. Moreover, the reconstruction of the FS's starts at T^* in detwinned $Ba(Fe_{1-x}Co_x)_2As_2$.[25] The discovery of this "electronic nematic phase" would indicate that the the ODW fluctuations develop divergently above T_S, and the structure transition is (almost) second-order.

Recently, prominent softening of the shear modulus in undoped and underdoped $Ba(Fe_{1-x}Co_x)_2As_2$ was reported by

acoustic measurements.[30,31] Yoshizawa *et al.*[31] observed all shear moduli C_{44}, C_{66}, and C_E. Recently, they also performed systematic measurement for $x = 0$–0.225, and found that only C_{66} shows prominent softening in both under- and overdoped systems.[32] Similar results were reported by Goto *et al.* independently.[33] This observation can be explained by the development of ferro-orbital fluctuations[10] or spin-nematic fluctuations.[30] Considering large quadrupole-strain coupling in iron pnictides, all the observations mentioned above suggest the importance of orbital physics, and pose a serious challenge for theories of iron pnictide superconductors. In fact, Goto *et al.* have shown that C_{66} is almost independent of the magnetic field up to ∼50 T, indicating the nonmagnetic origin of the softening.[33]

Thus, the main features of the iron-pnictide superconductors would be summarized as (i) the orthorhombic (or nematic) transition accompanied by remarkable C_{66} softening, (ii) the emergence of high-T_c superconductivity next to the orthorhombic phase, and (iii) the stripe-type magnetic order induced by the orthorhombicity. The unified explanation has not been achieved as far as we know.

In this paper, we develop the orbital fluctuation theory to explain the above-mentioned features (i)–(iii) based on the random-phase approximation (RPA) and beyond the RPA. In the RPA, large O_{xz}-antiferroquadrupole (AFQ) fluctuations are produced by the e-ph interactions, while they do not produce the softening of C_{66} or C_{44}. If we go beyond the RPA, however, we find that the $O_{x^2-y^2}$-ferroquadrupole (FQ) fluctuations are brought about by the "two-orbiton process" near the AFQ quantum-critical point (QCP). The induced FQ fluctuations cause the softening of C_{66}, and the commensurate ferro-orbital order is realized at $T = T_S$. It is predicted that the AFQ-QCP is located at the FQ-QCP, which is the end point of the orthorhombic phase. Near this multi-orbital QCP, the superconductivity is caused mainly by the AFQ fluctuations, and the orthorhombic transition is brought about by the FQ fluctuations. Moreover, the stripe-type antiferromagnetic state is induced in the orbital-ordered state, since the orbital polarization gives strong in-plane anisotropy in the spin-nesting. The present study gives a microscopic justification for the anisotropic Heisenberg model description in the SDW state.[26,34]

There is a long history in the study of superconductivity due to charge or orbital fluctuations in multi-orbital systems, starting from the exciton-assisted superconductivity.[35–39] In multi-orbital systems, on-site Coulomb interaction is composed of the intra-orbital term U, the interorbital one U', and Hund's or the exchange term J. Since U is usually larger than $U' \approx U - 2J$, spin fluctuations induced by U give non-s-wave SC states. However, Takimoto *et al.*[40] showed that charge (or orbital) fluctuations induced by U' give a conventional s-wave SC state if the relations $U' > U$ and $J \sim 0$ are assumed. Although this idea was applied to pnictides,[41] the relation $U' \sim 0.6U$ is realized in many compounds.[42] Even if $U' \sim 0.6U$ and $J \sim 0.2U$, the present authors have shown that the orbital-fluctuation-mediated superconductivity is realized by quadrupole-quadrupole interaction mediated by non-A_{1g} phonons, which works as the "negative effective exchange $J_{\rm eff}$ for the charge sector."[9] In iron pnictides, orbital fluctuations develop even when the dimensionless e-ph coupling λ due to Fe-ion optical phonons is just ∼0.2, according to the RPA[10] and FLEX approximation.[11] As for the As-ion A_{1g} mode,[41] orbital fluctuations develop only when $\lambda_{A_{1g}} \sim 1$, which is unrealistic in iron pnictides.

Recently, Yanagi *et al.*[43] added the "orthorhombic phonon" to the HH model proposed by the present authors,[9–11] and studied the ferro-orbital fluctuations. However, neither high-T_c nor structure transition are explained by their theory: First, the "orthorhombic-phonon" is acoustic ($\omega_{\boldsymbol{q}} \propto |\boldsymbol{q}|$), although it is treated as optical in Ref. 43 incorrectly. Their theory belongs to the cooperative Jahn-Teller structure transition due to acoustic phonons such as manganites; see details in Appendix A. In this case, the energy scale of "ferro-orbital fluctuations" is too low ($\sim\omega_{\boldsymbol{q}}$) to explain high-$T_c$, since T_c is much higher than $\omega_{\boldsymbol{q}} \sim 10$ K for $|\boldsymbol{q}| \sim 0.1\pi$.[44,45] Small orthorhombicity $(a-b)/(a+b) \sim 0.003$ in iron pnictides is also inconsistent with the cooperative Jahn-Teller scenario. Second, the derived orbital order is "incommensurate,"[46] which is inconsistent with the orthorhombic structure transition and the C_{66} softening.

These problems are resolved in the present theory since both high-energy AFQ and low-energy "commensurate" FQ fluctuations develop at the same time, without the necessity of fine-tuning model parameters. The former (latter) fluctuations give the superconductivity (orthorhombic transition).

II. MODEL HAMILTONIAN

First, we briefly explain the relation between five-orbital and ten-orbital models for iron pnictides. In this study, we set x and y axes parallel to the nearest Fe-Fe bonds, and represent the z^2, xz, yz, xy, and x^2-y^2 d orbitals in the xyz coordinate as 1, 2, 3, 4, and 5, respectively. The FS's are mainly composed of t_{2g} orbitals ($l = 2$–4), although e_g orbitals also play non-negligible roles in producing orbital fluctuations.[10] Figure 1 shows the crystal structure of the FeAs plane. Since the As-A (As-B) ions form the upper (lower) plane, the unit cell contains Fe-A and Fe-B, which we call the two-iron unit cell. Since each Fe ion contains five orbitals, the original tight-binding model for iron pnictides is given as the "ten-orbital model."

In Refs. 2 and 42, the authors introduced the gauge transformation $|2,3\rangle \to -|2,3\rangle$ only for Fe-B sites, which we call the "unfold gauge transformation." Due to this gauge transformation, the unit cell of the kinetic term is halved to become the single-iron unit cell, shown in Fig. 1. In the

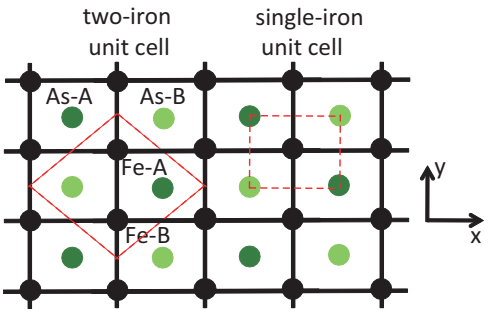

FIG. 1. (Color online) Crystal structure of the FeAs layer, in which the unit cell is given by the two-iron unit cell composed of Fe-A, Fe-B, As-A, and As-B. The single-iron unit cell is realized by applying the "unfold gauge transformation."

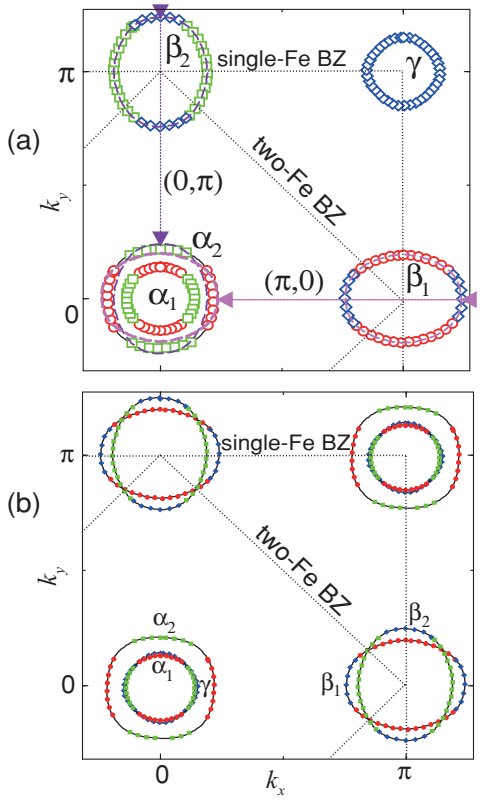

FIG. 2. (Color online) (a) FS's for $n = 6.0$ in the unfolded model. The colors correspond to 2 (green), 3 (red), and 4 (blue), respectively. The interorbital nesting between FS α_2 (green) and FS β_2 (blue) causes the AFQ fluctuations. (b) FS's for the original ten-orbital model.

obtained "five-orbital model," the kinetic term is given as

$$H_0 = \sum_{ij;lm;\sigma} t_{lm}^{ij} c_{i,l\sigma}^{\dagger} c_{j,m\sigma}, \tag{1}$$

where i,j denotes the unit cell, $l,m = 1$–5 represent the d orbital, and $\sigma = \pm 1$ is the spin index. $c_{i,l\sigma}^{\dagger}$ is the creation operator of the d electron, and t_{lm}^{ij} with $i \neq j$ $(i = j)$ is the hopping integral (local potential). This five-orbital model is convenient to study the Eliashberg gap equation.[2,9] In studying the orbital physics, however, we have to keep in mind the fact that the sign of the quadrupole operators $\hat{O}_{xz}$ and $\hat{O}_{yz}$ at the Fe-B sites is reversed by the unfold gauge transformation. By taking care of this fact, we study the softening of shear moduli based on the five-orbital model hereafter. In Appendix B, we calculate the orbital fluctuations using the original ten-orbital model, and make a comparison between the results of the two models.

Figure 2 shows the FS's in (a) the five-orbital model and (b) the ten-orbital model. The FS's in (a) coincide with the FS's in (b) if we fold the former FS's into the two-iron Brillouin zone (BZ). We use the hopping parameters for LaOFeAs given in Ref. 2. The colors correspond to 2 (green), 3 (red), and 4 (blue), respectively. The interorbital nesting between orbital 2 on FS α_2 and orbital 4 on FS β_2 causes the most divergent AFQ fluctuations.

Next, we introduce the e-ph interaction due to Fe-ion Einstein optical modes. The Hamiltonian given in Eq. (4) of Ref. 10 is simply rewritten as the following bilinear form in the xyz coordinate:

$$H_{e\text{-ph}} = \eta \sum_i \left(\hat{O}_{yz}^i u_x^i + \hat{O}_{xz}^i u_y^i + \hat{O}_{xy}^i u_z^i \right), \tag{2}$$

where $\eta = 60e^2 a_d^2 / 7\sqrt{3} R_{\text{Fe-As}}^4$; a_d is the radius of the d orbital (e.g., the Shannon crystal radius of Fe^{2+} is 0.77 Å), and $R_{\text{Fe-As}} \approx 2.4$ Å. $\boldsymbol{u}^i$ is the displacement vector of the ith Fe ion, and $\hat{O}_{\Gamma}^i$ $(\Gamma = xz, yz, xy)$ is the charge quadrupole operator given as

$$\hat{O}_{\Gamma}^i \equiv \sum_{lm}^{\pm} o_{\Gamma}^{l,m} \hat{m}_{l,m}^i, \tag{3}$$

where $\hat{m}_{l,m}^i \equiv \sum_{\sigma} c_{i,l\sigma}^{\dagger} c_{i,m\sigma}$, and the coefficient is defined as $o_{xz}^{l,m} = 7\langle l|\hat{x}\hat{z}|m\rangle$ for $\Gamma = xz$, where $\hat{\boldsymbol{x}} = x/r$ and so on. The nonzero coefficients are given as

$$o_{xz}^{2,5} = o_{xz}^{3,4} = \sqrt{3} o_{xz}^{1,2} = 1, \tag{4}$$

$$-o_{yz}^{3,5} = o_{yz}^{2,4} = \sqrt{3} o_{yz}^{1,3} = 1, \tag{5}$$

$$o_{xy}^{2,3} = -\sqrt{3} o_{xy}^{1,4} / 2 = 1. \tag{6}$$

Be careful not to confuse $\hat{O}_{xz}$ with the xz-orbital operator. The other two quadrupole operators are O_{z^2} and $O_{x^2-y^2}$, whose coefficients are, respectively, defined as $o_{x^2-y^2}^{l,m} = (7/2)\langle l|(\hat{x}^2 - \hat{y}^2)|m\rangle$ and $o_{z^2}^{l,m} = (7/2\sqrt{3})\langle l|(3\hat{z}^2 - 1)|m\rangle$. (They are written as O_2^0 and O_2^2 in the literature.) The nonzero coefficients are given as

$$o_{x^2-y^2}^{2,2} = -o_{x^2-y^2}^{3,3} = -(\sqrt{3}/2) o_{x^2-y^2}^{1,5} = 1, \tag{7}$$

$$o_{z^2}^{1,1} = 2o_{z^2}^{2,2} = 2o_{z^2}^{3,3} = -o_{z^2}^{4,4} = -o_{z^2}^{5,5} = 2/\sqrt{3}. \tag{8}$$

Except for $\Gamma = z^2$, all the matrix elements of $\hat{o}_{\Gamma}$ with respect to the t_{2g} orbital (2–4) are ± 1.

Here, we derived the e-ph interaction based on the point-charge model. Although e-ph interaction is also induced by the change in the d-p hopping, as discussed in Ref. 47, we expect it is small since the weight of the p electron on the Fermi surface is just $\sim 5\%$ in iron pnictides. Fortunately, because of the Wigner-Eckart theorem, the matrix elements of the local quadrupole-phonon interaction are always given by the quadrupole operator $\hat{O}_{\Gamma}^i$, independently of the details of the interaction. Since the magnitude of the hexadecapole-phonon interaction is $(a_d/R_{\text{Fe-Fe}})^2 \sim 0.1$ times that of the quadrupole-phonon interaction, we can safely use Eq. (2).

Equation (2) means that the displacement u_x produces the quadrupole potential $\hat{O}_{yz}$, which causes the scattering of electrons between orbitals 2 and 4. The e-ph interactions in Eq. (2) within t_{2g} orbitals are shown in Fig. 3. Then, the

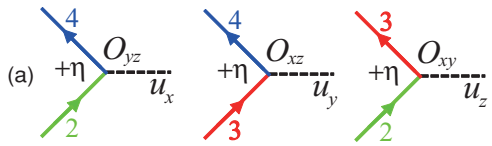

FIG. 3. (Color online) Interorbital scattering processes due to the e-ph interaction by u_{μ} $(\mu = x,y,z)$ within the t_{2g} orbitals $(l = 2$–$4)$.

phonon-mediated el-el interaction $V^{\rm ph}_{\rm el\text{-}el}$ is obtained by taking the contraction of $\boldsymbol{u}^i$, which gives the local phonon Green function $D(\tau) \equiv \langle T_\tau u^i_\mu(\tau) u^i_\mu(0)\rangle (\mu = x,y,z)$. By taking the Fourier transformation, we obtain

$$D(\omega_l) = \frac{2\langle u^2\rangle_0 \omega_D}{\omega_l^2 + \omega_D^2}, \tag{9}$$

where $\omega_l = 2\pi T l$ is the boson Matsubara frequency, ω_D is the optical phonon frequency, and $\sqrt{\langle u^2\rangle_0} = \sqrt{1/2M_{\rm Fe}\omega_D}$ is the uncertainty in position for Fe ions; $\sqrt{\langle u^2\rangle_0} = 0.044$ Å for $\omega_D = 0.02$ eV.[10] Then, $V^{\rm ph}_{\rm el\text{-}el}$ is expressed as the following quadrupole-quadrupole interaction:

$$V^{\rm ph}_{\rm el\text{-}el} = -g(\omega_l)\sum_i \left\{ \hat{O}^i_{yz}\cdot\hat{O}^i_{yz} + \hat{O}^i_{xz}\cdot\hat{O}^i_{xz} + \hat{O}^i_{xy}\cdot\hat{O}^i_{xy} \right\}, \tag{10}$$

where $g(\omega_l) = g\omega_D^2/(\omega_l^2+\omega_D^2)$, and g is the phonon-mediated el-el interaction at zero frequency; $g = 0.34$ eV in the present point-charge model.[9,10]

III. RANDOM-PHASE APPROXIMATION

Now we explain the RPA for the five-orbital HH model.[40] The irreducible susceptibility in the five-orbital model is given by

$$\chi^0_{ll',mm'}(q) = -\frac{T}{N}\sum_k G^0_{lm}(k+q)\, G^0_{m'l'}(k), \tag{11}$$

where $\hat{G}^0(k) = [i\epsilon_n + \mu - \hat{H}^0_{\boldsymbol{k}}]^{-1}$ is the d-electron Green function in the orbital basis, $q = (\boldsymbol{q},\omega_l)$, $k = (\boldsymbol{k},\epsilon_n)$, and $\epsilon_n = (2n+1)\pi T$ is the fermion Matsubara frequency. μ is the chemical potential and $\hat{H}^0_{\boldsymbol{k}}$ is the kinetic term. Then, the susceptibilities for spin and charge sectors in the RPA are given as[40]

$$\hat{\chi}^s(q) = \frac{\hat{\chi}^0(q)}{1-\hat{\Gamma}^s\hat{\chi}^0(q)}, \tag{12}$$

$$\hat{\chi}^c(q) = \frac{\hat{\chi}^0(q)}{1+\hat{\Gamma}^c(\omega_l)\hat{\chi}^0(q)}, \tag{13}$$

where the bare four-point vertices $\hat{\Gamma}^{s,c}$ are

$$\Gamma^s_{l_1l_2,l_3l_4} = \begin{cases} U, & l_1=l_2=l_3=l_4, \\ U', & l_1=l_3\neq l_2=l_4, \\ J, & l_1=l_2\neq l_3=l_4, \\ J', & l_1=l_4\neq l_2=l_3, \end{cases} \tag{14}$$

$$\hat{\Gamma}^c(\omega_l) = -\hat{C} - 2\hat{V}^{\rm ph}_{\rm el\text{-}el}(\omega_l), \tag{15}$$

$$C_{l_1l_2,l_3l_4} = \begin{cases} U, & l_1=l_2=l_3=l_4, \\ -U'+2J, & l_1=l_3\neq l_2=l_4, \\ 2U'-J, & l_1=l_2\neq l_3=l_4, \\ J', & l_1=l_4\neq l_2=l_3. \end{cases} \tag{16}$$

In Eq. (15), $(V^{\rm ph}_{\rm el\text{-}el})_{l_1,l_2,l_3,l_4} = -g(\omega_l)\sum_\Gamma^{xz,yz,yx} o^{l_1,l_2}_\Gamma o^{l_3,l_4}_\Gamma$. Here, we neglect the ladder diagram for phonon-mediated interaction because of the relation $\omega_D \ll W_{\rm band}$.[9]

In the RPA, the enhancement of the spin susceptibility $\hat{\chi}^s$ is mainly caused by the intra-orbital Coulomb interaction U, using the "intra-orbital nesting." On the other hand, the enhancement of $\hat{\chi}^c$ in the present model is caused by the phonon-induced quadrupole-quadrupole interaction in Eq. (10), utilizing the "interorbital nesting" in the present model. The SDW (ODW) state is realized when the spin (charge) Stoner factor $\alpha_{s(c)}$, which is the maximum eigenvalue of $\hat{\Gamma}^{s(c)}\hat{\chi}^0(\boldsymbol{q},0)$, is unity. When $n = 6.05$, the critical value of U is $U_c = 1.26$ eV, and the critical value of g (at $U = 0$) is $g_c = 0.233$ eV. The smallness of g_c in iron pnictides originates from the better interorbital nesting. Hereafter, we set the unit of energy as eV unless otherwise noted.

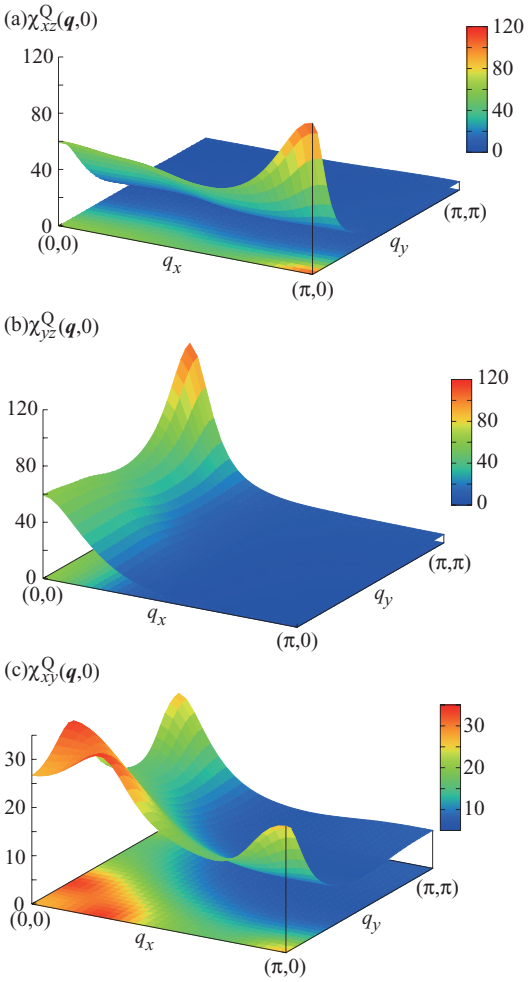

FIG. 4. (Color online) Quadrupole susceptibilities in the five-orbital model for (a) $\chi^Q_{xz}(\boldsymbol{q})$, (b) $\chi^Q_{yz}(\boldsymbol{q})$, and (c) $\chi^Q_{xy}(\boldsymbol{q})$, respectively. The used model parameters are $n = 6.05$, $T = 0.05$, and $g = 0.22$ ($\alpha_c = 0.98$). The correlation length in (a) or (b) is derived as $\xi = \pi/\Delta q \sim 3$, where Δq is the half-width of the peak. Therefore, we obtain the relations $6\xi^2 \sim (1-\alpha_c)^{-1}$ and $c\xi^2 \sim 2(1-\alpha_c)^{-1} \sim 12\xi^2$.

Here, we introduce the diagonal charge quadrupole susceptibilities in the five-orbital model as

$$\chi^Q_\Gamma(q) = \sum_{ll'}\sum_{mm'} o^{ll'}_\Gamma \chi^c_{ll'mm'}(q) o^{mm'}_\Gamma \tag{17}$$

for $\Gamma = xz,yz,xy$. Their momentum dependence at zero frequency is shown in Fig. 4 for $\alpha_c = 0.98$. More generally, the quadrupole susceptibility is defined as

$$\chi^Q_{\Gamma,\Gamma'}(q) = \sum_{ll'}\sum_{mm'} o^{ll'}_\Gamma \chi^c_{ll'mm'}(q) o^{mm'}_{\Gamma'}. \tag{18}$$

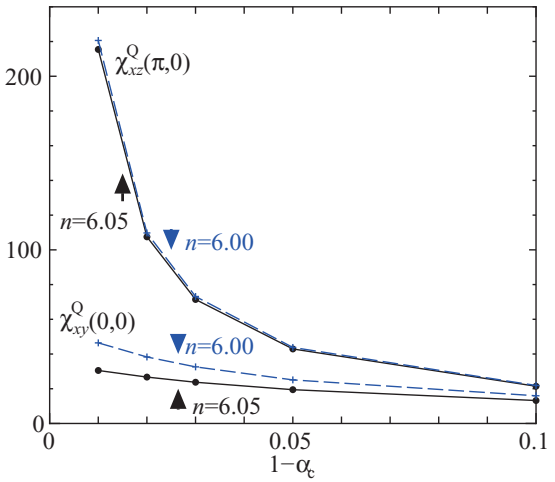

FIG. 5. (Color online) Quadrupole susceptibilities as a function of α_c for $n = 6.0$ and 6.05 given by the RPA. Model parameters are $U = 0.8$ and $T = 0.05$. We can recognize the relation $\chi^Q_{xz}(\boldsymbol{Q}) \propto (1-\alpha_c)^{-1} \propto (g_c - g)^{-1}$, which diverges at $\alpha_c = 1$ or $g = g_c$.

However, its off-diagonal terms with $\Gamma \neq \Gamma'$ are negligibly small in the present model in the "xyz coordinate." In this approximation, in the absence of Coulomb interaction, the quadrupole susceptibility in the RPA is given as

$$\chi^Q_\Gamma(q) \approx \chi^{Q,0}_\Gamma(q)/\left[1 - 2g\chi^{Q,0}_\Gamma(q)\right], \tag{19}$$

where $\chi^{Q,0}_\Gamma$ is the irreducible quadrupole susceptibility. Considering the fact that $\chi^0_{ll',mm'}(q)$ takes a large value for $l = m$ and $l' = m'$, we obtain $\chi^{Q,0}_{xz}(q) \approx 2\chi^0_{25,25}(q) + 2\chi^0_{34,34}(q) + (2/3)\chi^0_{12,12}(q)$. Since $\chi^{Q,0}_{xz}(q) \approx 2.5$ at $\boldsymbol{q} = (\pi,0)$, the critical value of g is $g_c \sim 0.2$ in the present model. We stress that the relations $\chi^Q_{\Gamma,\Gamma'}(q) = \chi^Q_\Gamma(q)\delta_{\Gamma,\Gamma'}$ and Eq. (19) hold exactly for $q = (\boldsymbol{0},\omega_l)$. We utilize this relation in calculating the shear modulus.

As for the contributions by t_{2g} orbitals ($l = 2$–4), $\chi^Q_{xz}(q) \propto \chi^c_{34,34}(q)$, $\chi^Q_{yz}(q) \propto \chi^c_{24,24}(q)$, and $\chi^Q_{xy}(q) \propto \chi^c_{23,23}(q)$. In Fig. 4(a), $\chi^Q_{xz}(\boldsymbol{q})$ has the highest peak at $\boldsymbol{q} = (\pi,0)$, which is given by the interorbital nesting between orbital 3 on FS α_2 and orbital 4 on FS β_1 in the five-orbital model in Fig. 2(a). Also, $\chi^Q_{yz}(\boldsymbol{q})$ has the highest peak at $\boldsymbol{q} = (0,\pi)$ in Fig. 4(b) due to the interorbital nesting between orbital 2 on FS α_2 and orbital 4 on FS β_2. We will see that $\chi^Q_{xz(yz)}(\boldsymbol{q})$ is modified by the unfolding procedure.

Also, $\chi^Q_{xy}(\boldsymbol{q})$ in Fig. 4(c) is given by the interorbital nesting between orbitals 2 and 3, due to the out-of-plane oscillations of Fe ions. The interband and intraband scattering processes produce the enhancement of $\chi^Q_{xy}(\boldsymbol{q})$ at $\boldsymbol{q} = (\pi,0),(0,\pi)$ and $\boldsymbol{q} = \boldsymbol{0}$, respectively. We note that $\chi^Q_{xy}(\boldsymbol{q})$ is not affected by the unfolding procedure.

Figure 5 shows both $\chi^Q_{xz}(\boldsymbol{q})$ at $\boldsymbol{q} = (\pi,0)$ and $\chi^Q_{xy}(\boldsymbol{0})$ as a function of α_c for $n = 6.0$ and 6.05 given by the RPA. We see that $\chi^Q_{xz}(\boldsymbol{q})$ develops divergently in proportion to $(1-\alpha_c)^{-1} \propto (g_c - g)^{-1}$, while $\chi^Q_{xy}(\boldsymbol{0})$ shows an enhanced but saturated value even at $g = g_c$.

In Appendix B, we will calculate $\chi^Q_\Gamma(q)$ in the ten-orbital model, and make a comparison to Fig. 4 in the five-orbital model: Although both results coincide for $\Gamma = xy, z^2, x^2 - y^2$, they are different for $\Gamma = xz, yz$. The reason is that the signs of $O_{xz/yz}$ at Fe-B sites are changed by applying the "unfold gauge transformation." As we will explain in Appendix B, the development of $\chi^Q_{xz/yz}(\boldsymbol{0},0)$ in Fig. 4 is the artifact of the unfold gauge transformation. For this reason, the correct AFQ susceptibility in the ten-orbital model is given as $\chi^Q_{xz/yz}(\boldsymbol{q}) = \chi^{Q,\text{five-orbital}}_{xz/yz}[\boldsymbol{q} + (\pi,\pi)]$. The optical modes that give the enhancements of $\chi^Q_{yz}(\boldsymbol{q})$ at $\boldsymbol{q} = (\pi,0)$ and (π,π) in the ten-orbital model [$\boldsymbol{q} = (0,\pi)$ and $(0,0)$ in the five-orbital model] are caused by the in-plane u_x oscillations shown in Fig. 6(a). Also, the enhancements of $\chi^Q_{xy}(\boldsymbol{q})$ at $\boldsymbol{q} = (\pi,0)$ and $(0,0)$ are caused by the out-of-plane u_z oscillations in Fig. 6(b).

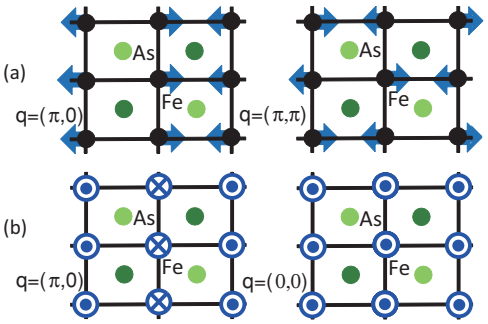

FIG. 6. (Color online) (a) Fe-ion in-plane optical phonons with momentum $\boldsymbol{q} = (\pi,0)$ and (π,π). (b) Fe-ion out-of-plane optical phonons with momentum $\boldsymbol{q} = (\pi,0)$ and $(0,0)$.

IV. ACOUSTIC PHONONS

In previous sections, we studied the e-ph interaction due to optical phonons, and calculated the quadrupole susceptibilities by the RPA. To obtain the shear modulus, we also must have knowledge of the e-ph interaction due to acoustic phonons with momentum $\boldsymbol{q} \approx 0$. In fact, shear modulus is proportional to the square of the acoustic phonon velocity, which is renormalized by the electron–acoustic-phonon interaction in the presence of strong quadrupole fluctuations. In this section, we derive the e-ph interaction due to acoustic phonons with $\boldsymbol{q} \approx 0$. Hereafter, we use the unit $\hbar = 1$, and take the nearest-neighbor Fe-Fe distance $a_{\text{Fe-Fe}}$ as the unit of length.

Figure 7 shows the transverse acoustic modes that are related to (a) C_{44}, (b) $C_E = (C_{11} - C_{12})/2$, and (c) C_{66}.[31] Now, we calculate the e-ph interaction based on the point-charge model by following the procedure in Ref. 9 for the optical phonons. The quadrupole potential energies at the Fe site caused by the transverse acoustic phonons in Fig. 7 are given as

$$V_{44} = -\frac{3e^2}{R^4_{\text{Fe-As}}}\frac{8}{\sqrt{3}}xz \cdot \tilde{u}_{44}, \tag{20}$$

$$V_E = -\frac{3e^2}{R^4_{\text{Fe-As}}}\frac{8}{\sqrt{3}}xy \cdot \tilde{u}_E, \tag{21}$$

$$V_{66} = \frac{3e^2}{R^4_{\text{Fe-As}}}\sqrt{6}(x^2 - y^2) \cdot \tilde{u}_{66} \tag{22}$$

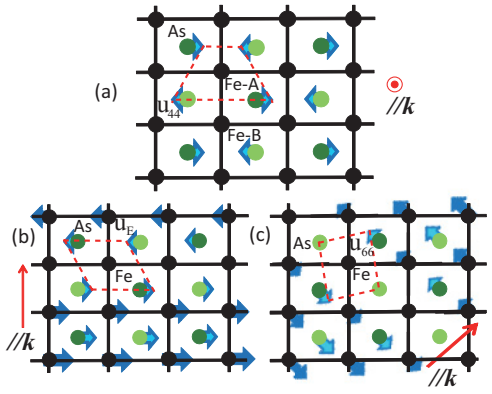

FIG. 7. (Color online) Displacement vectors $\boldsymbol{u}_{\rm As}$ and $\boldsymbol{u}_{\rm Fe}$ in the transverse acoustic modes that couple with (a) C_{44}, (b) C_E, and (c) C_{66}. The C_{66} mode corresponds to the orthorhombic structure transition.

for both Fe-A and Fe-B sites, where (x,y,z) are the coordinates of the d electron. $\tilde{\boldsymbol{u}}_\phi \equiv \boldsymbol{u}_\phi - \boldsymbol{u}_{\rm Fe}$ $(\phi = 44, 66, E)$ is the relative displacements of the nearest As ions from the center Fe ion; u_ϕ $(u_{\rm Fe})$ is the displacement vector of the As (Fe) ion we are considering from the original position. Note that the shear strain tensors are given as $\epsilon_{44(E)} = \tilde{u}_{44(E)}/(a_{\text{Fe-Fe}}/2) = 2\tilde{u}_{44(E)}$ and $\epsilon_{66} = \tilde{u}_{66}/(a_{\text{Fe-Fe}}/\sqrt{2}) = \sqrt{2}\tilde{u}_{66}$.

The corresponding operators in the ten-orbital model are given, respectively, as

$$\hat{V}_{44} = -\frac{3e^2a_d^2}{R_{\text{Fe-As}}^4}\frac{8}{7\sqrt{3}}\hat{O}_{xz}\cdot\tilde{u}_{44}, \tag{23}$$

$$\hat{V}_E = -\frac{3e^2a_d^2}{R_{\text{Fe-As}}^4}\frac{8}{7\sqrt{3}}\hat{O}_{xy}\cdot\tilde{u}_E, \tag{24}$$

$$\hat{V}_{66} = \frac{3e^2a_d^2}{R_{\text{Fe-As}}^4}\frac{2\sqrt{6}}{7}\hat{O}_{x^2-y^2}\cdot\tilde{u}_{66}. \tag{25}$$

Therefore, the acoustic modes in Figs. 7(a)–7(c) couple with the quadrupole susceptibilities at $\boldsymbol{q} \approx 0$; $\chi^Q_{xz}(0)$, $\chi^Q_{xy}(0)$, and $\chi^Q_{x^2-y^2}(0)$ for $\phi = 44$, E, and 66 in the ten-orbital model, respectively.

To study the softening in the five-orbital models, we have to perform the "unfold gauge transformation" for Eqs. (23)–(25). Under the gauge transformation, Eqs. (24) and (25) are invariant, while Eq. (23) is changed to

$$\hat{V}'_{44} = \mp\frac{3e^2a_d^2}{R_{\text{Fe-As}}^4}\frac{8}{7\sqrt{3}}\hat{O}_{xz}\cdot\tilde{u}_{44}, \tag{26}$$

where the $-$ $(+)$ sign corresponds to the Fe-A (Fe-B) site. In the "five-orbital model," therefore, the softening of C_E and C_{66} is caused by $\chi^Q_{xy}(\boldsymbol{0},0)$ and $\chi^Q_{x^2-y^2}(\boldsymbol{0},0)$, respectively, while the softening of C_{44} is caused by $\chi^Q_{xz}((\pi,\pi),0)$. Therefore, the softening in the shear modulus (C_{66} and C_{44}) does not occur within the RPA.[48]

Next, we derive the effective el-el interaction due to $\boldsymbol{k} \to 0$ transverse acoustic modes. In the case of $\boldsymbol{k} = k(1,1)/\sqrt{2}$ and $k \ll 1$ shown in Fig. 7(c), the displacement operator for the As site at $\boldsymbol{R}_s$ is

$$u_s = \sum_{\boldsymbol{k}}\sqrt{\frac{1}{2NM\omega_{\boldsymbol{k}}}}\left[a_{\boldsymbol{k}}e^{i\boldsymbol{k}\cdot\boldsymbol{R}_s} + a^\dagger_{\boldsymbol{k}}e^{-i\boldsymbol{k}\cdot\boldsymbol{R}_s}\right], \tag{27}$$

where $a_{\boldsymbol{k}}$ and $a^\dagger_{\boldsymbol{k}}$ satisfy the commutation relation $[a_{\boldsymbol{k}}, a^\dagger_{\boldsymbol{k}'}] = \delta_{\boldsymbol{k},\boldsymbol{k}'}$, M is the mass of the As ion, and $\omega_{\boldsymbol{k}} = v_{\boldsymbol{k}}|\boldsymbol{k}|$; $v_{\boldsymbol{k}}$ is the bare acoustic phonon velocity. The Fourier transformation of u_s is given as $u_{\boldsymbol{k}} = \sqrt{\frac{1}{2M\omega_{\boldsymbol{k}}}}(a_{\boldsymbol{k}} + a^\dagger_{-\boldsymbol{k}})$. Then, the Fourier transformation of the acoustic-phonon Green function $D_{\boldsymbol{k}}(\tau) \equiv \langle T_\tau u^i_{\boldsymbol{k}}(\tau)u^i_{\boldsymbol{k}}(0)\rangle$ is

$$D_{\boldsymbol{k}}(\omega_n) = \frac{2\omega_{\boldsymbol{k}}}{\omega_n^2 + \omega_{\boldsymbol{k}}^2}\langle u^2_{\boldsymbol{k}}\rangle_0, \tag{28}$$

where $\langle u^2_{\boldsymbol{k}}\rangle_0 = (1/2M\omega_{\boldsymbol{k}})$.

As understood in Fig. 7(c), the relative displacement with the origin at the Fe ion, $\tilde{u}_s$, is given as $\frac{1}{2}(u_{s'} - u_s)$, where $\boldsymbol{R}_{s'} = (0.5,0.5)$ and $\boldsymbol{R}_s = (-0.5,-0.5)$ with the origin at the Fe ion. Considering that $(\boldsymbol{R}_{s'} - \boldsymbol{R}_s)\cdot\boldsymbol{k} = \sqrt{2}k$, its Fourier transformation is given as

$$\tilde{u}_{\boldsymbol{k}} \equiv \sum_s \tilde{u}_s e^{-i\boldsymbol{k}\cdot\boldsymbol{R}_s} \sim \frac{ik}{\sqrt{2}}u_{\boldsymbol{k}}. \tag{29}$$

To calculate the shear modulus, we need the quadrupole susceptibility in the "k limit," in which we set $\omega = 0$ first, and take the limit $k \to 0$ later.[49] For this purpose, we derive the effective el-el interaction due to the transverse acoustic phonon in the k limit. The el-el interaction due to the phonon in Fig. 7(c) is given by the second-order term of Eq. (25). Using the relation $D_{\boldsymbol{k}}(0)\boldsymbol{k}^2 = 2(1/2M\omega_{\boldsymbol{k}})\boldsymbol{k}^2/\omega_{\boldsymbol{k}} = 1/Mv^2_{\boldsymbol{k}}$, it is given as

$$H_{66} = -g_{66}\sum_{\boldsymbol{k}\boldsymbol{k}',ll'mm',\sigma\sigma'} o^{ll'}_{x^2-y^2}o^{mm'}_{x^2-y^2} \times c^\dagger_{l\boldsymbol{k}\sigma}c_{l'\boldsymbol{k}\sigma}c^\dagger_{m\boldsymbol{k}'\sigma'}c_{m'\boldsymbol{k}'\sigma'}, \tag{30}$$

$$g_{66} = \frac{B^2}{R^2_{\text{Fe-As}}}\frac{1}{Mv^2_{\boldsymbol{k}}}, \tag{31}$$

where $B \equiv \frac{3e^2}{R_{\text{Fe-As}}}(\frac{a_d}{R_{\text{Fe-As}}})^2\frac{2\sqrt{3}}{7}$; $B = 0.95$ eV for $a_d = 0.77$ Å (which is the Shannon crystal radius of Fe^{2+}) and $R_{\text{Fe-As}} = 2.4$ Å. Therefore,

$$g_{66} = \eta^2_{66}C^{-1}_{66,0}, \tag{32}$$

where $C_{66,0} \equiv Mv^2_{\boldsymbol{k}}$ is the bare shear modulus and $\eta_{66} = BR^{-1}_{\text{Fe-As}}$ is the quadrupole-strain coupling constant. If we set $v_{\boldsymbol{k}} \sim 0.024$ eV Å ($v_{\boldsymbol{k}} \sim 0.018$ eV Å) according to the first-principles study,[50] we obtain $g_{66} = 0.12$ eV ($g_{66} = 0.21$ eV). On the other hand, we obtain $g = 0.34$ eV for the Fe-ion optical phonons with $\omega_D = 0.02$ eV.[10] Thus, $g_{66}/g = 1/2 \sim 1/3$ in the present point charge model.

In the same way, we also derive the el-el interactions due to the acoustic phonon with $\boldsymbol{k} = k(0,1)$, shown in Fig. 7(b). For this mode, the relative displacement $\tilde{u}_{\boldsymbol{k}}$ is given as $\tilde{u}_s \equiv$

$\frac{1}{2}(u_{s'} - u_s)$ with $\boldsymbol{R}_{s'} = (0.5,0.5)$ and $\boldsymbol{R}_s = (0.5, -0.5)$. Since $(\boldsymbol{R}_{s'} - \boldsymbol{R}_s) \cdot \boldsymbol{k} = k$, its Fourier transformation is given by

$$\bar{u}_{\boldsymbol{k}} \equiv \sum_s \tilde{u}_s e^{-i\boldsymbol{k}\cdot\boldsymbol{R}_s} \sim \frac{ik}{2} u_{\boldsymbol{k}}. \tag{33}$$

Then, the phonon-mediated el-el interactions are given by the second-order terms of Eq. (24). As a result, the el-el interactions due to phonons in Fig. 7(b) are given as

$$H_E = -g_E \sum_{\boldsymbol{k}\boldsymbol{k}',ll'mm',\sigma\sigma'} o_{xy}^{ll'} o_{xy}^{mm'} c_{l\boldsymbol{k}\sigma}^{\dagger} c_{l'\boldsymbol{k}\sigma} c_{m\boldsymbol{k}'\sigma'}^{\dagger} c_{m'\boldsymbol{k}'\sigma'}, \tag{34}$$

where $g_E = \frac{B'^2}{R_{\text{Fe-As}}^2} \frac{1}{M v_{\boldsymbol{k}}^2}$ and $B' \equiv \frac{3e^2}{R_{\text{Fe-As}}} (\frac{a_d}{R_{\text{Fe-As}}})^2 \frac{4}{7\sqrt{3}}$. In the same way, we obtain $g_{44} = g_E$. Therefore, $g_\phi = \eta_\phi^2 C_{\phi,0}^{-1}$ and $\eta_\phi^2 = 0.44\eta_{66}^2$ for $\phi = 44, E$. In conclusion, $g_E = g_{44} = 0.44 g_{66}$ if $v_{\boldsymbol{k}}$ is equivalent for all modes.

V. SOFTENING OF SHEAR MODULI

A. Softening due to the one-orbiton process; the RPA

Here, we calculate the shear modulus given by the one-orbiton process using the RPA. For this purpose, we introduce the following shear modulus susceptibilities in the five-orbital model, in the absence of e-ph interaction due to the $\boldsymbol{q} \approx 0$ acoustic phonon:

$$\chi_E = 2\chi_{xy}^{Q}(\boldsymbol{0},0), \tag{35}$$

$$\chi_{44} = 2\chi_{xz}^{Q}((\pi,\pi),0), \tag{36}$$

$$\chi_{66} = 2\chi_{x^2-y^2}^{Q}(\boldsymbol{0},0), \tag{37}$$

where the factor 2 comes from the spin degeneracy. They are schematically depicted in Fig. 8(a). Note that $\chi_{44} = 2\chi_{xz}^{Q}(\boldsymbol{0},0)$ in the ten-orbital model. According to Sec. 2 in Ref. 51, the shear modulus is given by the second derivative of the free energy with respect to the shear strain tensor: The expression for the shear modulus C_ϕ ($\phi = E, 44, 66$) is[51,52]

$$C_\phi = C_{\phi,0} - \eta_\phi^2 \chi_\phi, \tag{38}$$

where $C_{\phi,0} = v_\phi^2 \rho$ is the bare shear modulus, where v_ϕ is the bare acoustic phonon velocity and ρ is the mass density. η_ϕ is the quadrupole-strain coupling constant due to the "acoustic phonon" given in Sec. IV. In Eq. (38), the condition for the structure transition, $C_\phi = 0$, is satisfied when $\chi_\phi = g_\phi^{-1} (\gg 1)$. That is, the structure transition occurs prior to the divergence of χ_ϕ.

We can rewrite the expression for C_ϕ given in Eq. (38) as follows:

$$C_\phi^{-1} = C_{\phi,0}^{-1}[1 + g_\phi \tilde{\chi}_\phi], \tag{39}$$

$$\tilde{\chi}_\phi = \chi_\phi/(1 - g_\phi \chi_\phi), \tag{40}$$

where $g_\phi \equiv \eta_\phi^2 C_{\phi,0}^{-1}$ is the effective el-el interaction due to acoustic phonons given in the previous section. In Eq. (39), the condition $C_\phi = 0$ corresponds to the divergence of $\tilde{\chi}_\phi$, since $\tilde{\chi}_\phi$ is the *total susceptibility* including the e-ph interactions due to acoustic phonons.

If we set $U = 0$ for simplicity, Eq. (40) is expressed as

$$\tilde{\chi}_{44} = \chi_{44}^0 / \left[1 - (g + g_{44})\chi_{44}^0\right], \tag{41}$$

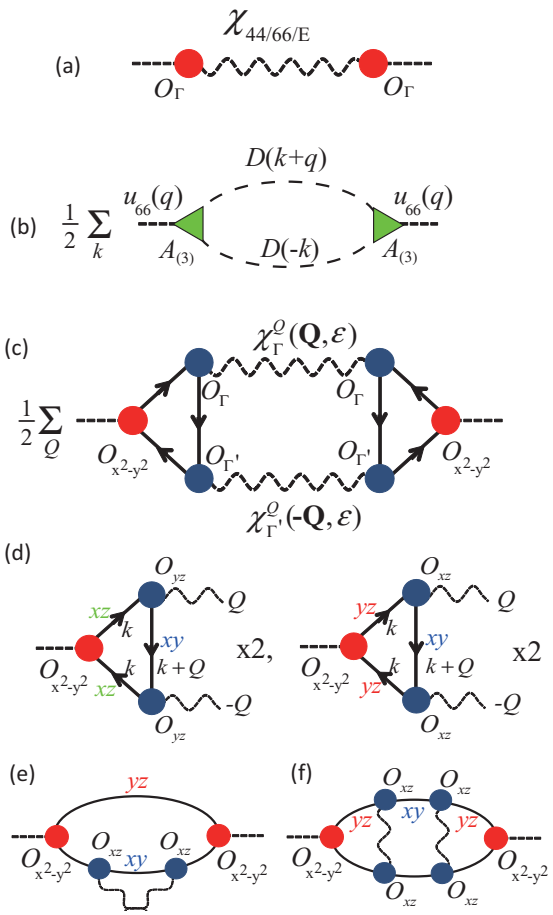

FIG. 8. (Color online) (a) Diagrammatic expression for the shear modulus susceptibilities χ_ϕ ($\phi = 44, 66, E$) in the RPA. (b) The second-order term with respect to the third-order anharmonic phonon-phonon interaction $A_{(3)} u_x^2 u_{66}$. This diagram represents the virtual process in which an acoustic phonon with $\boldsymbol{q} = 0$ breaks into two optical phonons conserving the total momentum. (c) Two-orbiton term for the shear modulus susceptibilities χ_{66}^{TO}, which is the irreducible susceptibility of $\chi_{x^2-y^2}(\boldsymbol{0},0)$. This term gives the softening of C_{66}. (d) Dominant contribution for the three-point vertex $A_{x^2-y^2}(\Gamma,\Gamma;\boldsymbol{q})$ for $\Gamma = xz$ and yz. (e) Self-energy correction due to $\chi_{xz}^Q(q)$. (f) Second-order Maki-Thompson-type vertex correction with respect to $\chi_{xz}^Q(q)$.

$$\tilde{\chi}_E = \chi_E^0 / \left[1 - (g + g_E)\chi_E^0\right], \tag{42}$$

$$\tilde{\chi}_{66} = \chi_{66}^0 / \left(1 - g_{66}\chi_{66}^0\right), \tag{43}$$

where the suffix 0 represents the bare susceptibility. According to $\tilde{\chi}_{44}$ in Eq. (41), g in Eq. (19) for χ_{xz}^Q is replaced with $g + g_{44}$ when both optical and acoustic phonons are taken into account. Therefore, we have to reduce g to $g - g_{44}$ to keep the charge Stoner factor α_c and $\chi_{xz}^Q(\boldsymbol{Q})$ unchanged. Considering the relation $g_{44} \sim g_E$ that we derived in the previous section, we obtain $\tilde{\chi}_E \sim \chi_E$. Then, we conclude that (i) $C_{44} \sim C_{44,0}$ since χ_{44} is seldom enhanced in the RPA. Also, (ii) C_E softens to some extent since $\chi_{xy}^Q(\boldsymbol{0})$ is weakly enhanced as shown in Fig. 5, although the relation $C_E = 0$ will not be satisfied because of the relation $\tilde{\chi}_E \sim \chi_E$.

As for C_{66} given in Eq. (43), χ^0_{66} in the present model is ~ 2 eV^{-1}, while we estimate $g_{66} = 0.1$–0.2 eV. Therefore, we expect (iii) $C_{66} \sim C_{66,0}$ in the RPA, which is inconsistent with experimentally observed large softening in C_{66}.[31] In the RPA, the softening in the shear modulus (C_{66}, C_{44}, and C_E) is small according to Eqs. (35)–(37) and Figs. 4(a)–4(c). In the next subsection, we analyze χ_{66} by taking into account the two-orbiton process, which is not included in the RPA.

B. Softening due to the two-orbiton process; the Aslamazov-Larkin-type diagram

In the previous subsection, we studied the softening of shear moduli within the RPA. However, the obtained softening is very small since only the AFQ fluctuations develop in the present model. In this subsection, we analyze χ_{66} by taking into account the "two-orbiton process," which is not included in the RPA. In usual cases, this higher-order process is negligible. However, it gives divergent increase in χ_{66}, and creates the FQ-QCP near the AFQ-QCP. For this reason, the orthorhombic structure transition ($C_{66} = 0$) is induced by the two-orbiton process.

Before calculating the two-orbiton process, let us consider the third-order anharmonic phonon-phonon coupling $\sim A_{(3)} u_x^2 u_{66}$, where u_x is the displacement of the Fe-ion optical mode in Eq. (2), and u_{66} is the displacement of the As-ion acoustic node in Eq. (22) or Eq. (25). Figure 8(b) shows the second-order-term with respect to $A_{(3)}$, where $D(q)$ is the optical phonon Green function in Eq. (9), and the factor $1/2$ is introduced to cancel the overcounting with respect to the upside-down diagrams. This term gives a self-energy correction for the acoustic phonon Green function. This two-phonon process would be measurable in Raman spectroscopy. By considering the e-ph interaction, each $D(q)$ in (b) is replaced with $D(q) + [\eta D(q)]^2 \chi^Q_{yz}(q)$.

Here, we study the ferroquadrupole susceptibility due to the "two-orbiton term" given by Fig. 8(c), and analyze for the softening of C_{66}. Since the coefficient of the anharmonic phonon-phonon coupling $A_{(3)}$ would be small in iron pnictides, we consider instead the three-point vertex given by the electron Green functions in Fig. 8(d). The two-orbiton term in Fig. 8(c) is similar to the Aslamazov-Larkin (AL) term for the excess conductivities due to superconducting fluctuations, such as longitudinal[53] and Hall[54] conductivities, and the Nernst coefficient.[55] Figure 8(c) is a virtual process in which one $O_{x^2-y^2}$-type orbiton with $\boldsymbol{q} = 0$ breaks into two O_{xz}-type orbitons with zero total momentum ($\pm \boldsymbol{Q}$). After taking the momentum summation, the two-orbiton term (c) in 2D systems would be strongly enhanced for $\boldsymbol{q} = 0$ since $\chi^Q_{yz}(\boldsymbol{k})$ has a large peak at finite momentum $\boldsymbol{k}$. The mathematical expression for the two-orbiton process in Fig. 8(c) for χ_{66}, which we call $\chi^{\rm TO}_{66}$, is given as

$$\chi^{\rm TO}_{66} = \frac{1}{2}(2g)^2 T \sum_{\boldsymbol{q},l,\Gamma,\Gamma'} A_{x^2-y^2}(\Gamma,\Gamma';\boldsymbol{q},\omega_l) A_{x^2-y^2}(\Gamma,\Gamma';\boldsymbol{q},\omega_l) \times \left[1 + 2g\chi^Q_{\Gamma}(\boldsymbol{q},\omega_l)\right]\left[1 + 2g\chi^Q_{\Gamma'}(\boldsymbol{q},\omega_l)\right]$$

$$\approx \frac{1}{2}(2g)^4 T \sum_{\boldsymbol{q},l,\Gamma,\Gamma'} A_{x^2-y^2}(\Gamma,\Gamma';\boldsymbol{q},\omega_l) A_{x^2-y^2}(\Gamma,\Gamma';\boldsymbol{q},\omega_l) \times \chi^Q_{\Gamma}(\boldsymbol{q},\omega_l)\chi^Q_{\Gamma'}(\boldsymbol{q},\omega_l), \quad (44)$$

where $A_{x^2-y^2}(\Gamma,\Gamma';\boldsymbol{q},\omega_l)$ is the three-point vertex with respect to $\hat{V}_{66}$ in Eq. (25) and quadrupole operators $\hat{O}_\Gamma$ and $\hat{O}_{\Gamma'}$, shown in Fig. 8(d). We used the relation $\chi^Q_\Gamma(q) = \chi^Q_\Gamma(-q)$. When $U = 0$, $A_{x^2-y^2}$ for $\omega_l = 0$ is given as

$$A_{x^2-y^2}(\Gamma,\Gamma';\boldsymbol{q}) = -2T \sum_{n,\boldsymbol{k}} \mathrm{Tr}\{\hat{G}_{\boldsymbol{k}}(\epsilon_n)\hat{o}_{x^2-y^2}\hat{G}_{\boldsymbol{k}}(\epsilon_n) \times \hat{o}_\Gamma \hat{G}_{\boldsymbol{k}+\boldsymbol{q}}(\epsilon_n)\hat{o}_{\Gamma'}\}, \quad (45)$$

where the factor 2 in front of Eq. (45) accounts for the diagrams with reversing three Green functions $\hat{G}_{\boldsymbol{k}}(\epsilon_n) \to \hat{G}_{-\boldsymbol{k}}(-\epsilon_n)$. Near the QCP $g \lesssim g_c$, the most divergent quadrupole susceptibility is $\chi^Q_{xz(yz)}$. Therefore, the dominant contribution for $\chi^{\rm TO}_{66}$ in Eq. (44) will be given by the term with $\Gamma = \Gamma' = xz$ or yz. After the analytic continuation, the functional form of $\chi^Q_{xz/yz}(\boldsymbol{q},\omega)$ for $\boldsymbol{q} \approx \boldsymbol{Q}_{xz} = (\pi,0)$ or $\boldsymbol{q} \approx \boldsymbol{Q}_{yz} = (0,\pi)$ would be approximately given as

$$\chi^Q_\Gamma(\boldsymbol{q},\omega + i\delta) = \frac{c\xi^2}{1 + \xi^2(\boldsymbol{q} - \boldsymbol{Q}_\Gamma)^2 - i\omega/\omega_0} \quad (46)$$

for $\Gamma = xz$ or yz, where ξ is the correlation length and ω_0 is the characteristic energy of the fluctuation. The relation $\xi^2 \propto \omega_0^{-1}$ holds in the RPA.

Next, we consider the temperature dependence of ξ. In the FLEX approximation[11] or SCR theory,[56] the bare susceptibility χ^0_ϕ is approximately suppressed as $\chi^0_\phi - \alpha T$ ($\alpha > 0$) due to the thermal fluctuations, which are described as the self-energy and Maki-Thompson vertex corrections. In this case, we obtain $\chi^Q_{xz}(\boldsymbol{Q},0) \propto [1 - g\chi^0_{xz}(\boldsymbol{Q},0) + g\alpha T]^{-1} \propto (T - T_{\rm AFQ})^{-1}$ based on the RPA, where $T_{\rm AFQ} = -[1 - g\chi^0_{xz}(\boldsymbol{Q},0)]/g\alpha$ is the transition temperature to the AFQ ordered state. Since $\chi^Q_{xz}(\boldsymbol{Q},0) \propto \xi^2$, we assume the following relations:

$$\xi^2 = l(T - T_{\rm AFQ})^{-1}, \quad (47)$$

$$\omega_0 = l'(T - T_{\rm AFQ}), \quad (48)$$

where l, l' are constants. Note that $\omega_0\xi^2$ is temperature-independent.[56] By carrier doping, $T_{\rm AFQ}$ changes from positive to negative, while other model parameters (c, l, and l') would be insensitive to doping. As shown in Fig. 5, $\chi^Q_{xz}(\boldsymbol{Q},0) \sim 2.4 \times (1 - \alpha_c)^{-1} \sim 12\xi^2$. In the case (i) $T_{\rm AFQ} > 0$, the relation $\omega_0 < T$ is satisfied near $T_{\rm AFQ}$. In the opposite case (ii) $T_{\rm AFQ} < 0$, the relation $\omega_0 > T$ will hold for a wide range of temperatures. Note that the present phenomenological model in Eqs. (46)–(48) is reproduced by the microscopic calculation by the FLEX approximation.[11] As for the spin propagator in cuprate superconductors, the relation $\omega_0 > T$ ($\omega_0 < T$) holds in overdoped (underdoped) systems.

Here, we comment on the self-energy correction and the Maki-Thompson-type vertex correction for $\chi^{\rm TO}_{66}$, shown in Figs. 8(e) and 8(f), respectively. The former term is included in the FLEX approximation, and it gives the Curie-Weiss behavior of $\chi^Q_{xz}(\boldsymbol{Q},0)$ given by Eqs. (46)–(48), as reported in Ref. 11 or Ref. 56. The latter term would be negligible since its temperature dependence is smaller than that of the former

TABLE I. Three-point vertex $A_\Gamma(xz,xz,\boldsymbol{Q})$ for $\Gamma = x^2-y^2$, xz, yz, and xy. $\boldsymbol{Q}=(\pi,0)$ corresponds to the peak position of $\chi^Q_{xz}(\boldsymbol{q},0)$ in the five-orbital model. We recognize that $A_\Gamma(xz,xz,\boldsymbol{Q}) \sim O(1)$ only for $\Gamma = x^2-y^2$; this selection rule means that $\chi^{\rm TO}_{44,E} \ll 1$.

Γ	x^2-y^2	xz	yz	xy
$A_\Gamma(xz,xz,\boldsymbol{Q})$	-0.60	1.9×10^{-3}	-1.0×10^{-3}	3.2×10^{-4}

term. For this reason, we concentrate on the two-orbiton term in Fig. 8(c) hereafter.

From now on, we perform the numerical calculation of the two-orbiton process in the case (i), in which the relations $\xi \gg 1$ and $\omega_0 \ll T$ are realized near the orbital-ordered state. In this case, the dominant contribution in Eq. (44) comes from the terms with $\Gamma = \Gamma' = xz$ and yz. Also, we can safely apply the classical approximation, in which the terms with $\omega_l \neq 0$ are dropped in Eq. (44). Under these approximations, Eq. (44) is simplified as

$$\chi^{\rm TO}_{66} = (2g)^4 T \sum_{\boldsymbol{q}} \left\{ A_{x^2-y^2}(xz,xz;\boldsymbol{q}) \chi^Q_{xz}(\boldsymbol{q},0) \right\}^2. \quad (49)$$

To calculate $A_{x^2-y^2}(\Gamma,\Gamma';\boldsymbol{q})$, we introduce a uniform FQ potential term $H' = h\sum_i \hat{O}^i_{x^2-y^2}$, where h is an infinitesimally small constant. Then, the three-point vertex is given as the following Ward identity:[57]

$$A_{x^2-y^2}(\Gamma,\Gamma';\boldsymbol{q}) = \frac{1}{h}\left[\bar{\chi}^Q_{\Gamma,\Gamma'}(\boldsymbol{q},0;h) - \bar{\chi}^Q_{\Gamma,\Gamma'}(\boldsymbol{q},0;0)\right], \quad (50)$$

where $\bar{\chi}^Q_{\Gamma,\Gamma'}(\boldsymbol{q},\omega_l;h)$ is the "irreducible" quadrupole susceptibility with respect to g. In the numerical calculation, we have to fix μ against the change in h. Equation (50) gives the correct three-point vertex even for $U \neq 0$. In the case of $U=0$, $\bar{\chi}^Q_{\Gamma,\Gamma'}$ is simply given as $\bar{\chi}^Q_{\Gamma,\Gamma'}(\boldsymbol{q},\omega_l;h) = -T\sum_{\boldsymbol{k},n} {\rm Tr}\{\hat{o}_\Gamma \hat{G}(\boldsymbol{k}+\boldsymbol{q},\epsilon_n+\omega_l;h)\hat{o}_{\Gamma'}\hat{G}(\boldsymbol{k},\epsilon_n;h)\}$. The obtained $A_{x^2-y^2}(xz,xz;\boldsymbol{q})$ for $U=0$ is presented in Fig. 9(a). A similar result is obtained for $U=0.8$ eV.

According to the functional form of $\chi^Q_{xz}(\boldsymbol{q},0)$ in Eq. (46), $\chi^{\rm TO}_{66}/T \propto \sum_{\boldsymbol{q}}\{\chi^Q_{xz}(\boldsymbol{q},0)\}^2 \propto \xi^2 \propto (T-T_{\rm AFQ})^{-1}$ in two-dimensional systems. The numerical result for $\chi^{\rm TO}_{66}/T$ given in Eq. (49) is shown in Fig. 9(b). The obtained result follows the relation $\chi^{\rm TO}_{66}/T \sim 0.1(1-\alpha_c)^{-1}$. Since $6\xi^2 \sim (1-\alpha_c)^{-1}$, the relation $\chi^{\rm TO}_{66}/T \sim 0.6\xi^2$ is verified numerically.

In the same way, two-orbiton processes for two other shear modulus susceptibilities, $\chi^{\rm TO}_{44}$ and $\chi^{\rm TO}_E$, are proportional to the square of $A_\Gamma(xz,xz;\boldsymbol{q})$ for $\Gamma = xz$ and xy, respectively. However, they are four orders of magnitude smaller than $\chi^{\rm TO}_{66}$, as recognized in Table I: This selection rule for A_Γ is understood as follows: According to the relation ${\rm Tr}\{\hat{O}_\Gamma \hat{O}_{xz}\hat{O}_{xz}\} = 0$ for $\Gamma = xz,xy$, we recognize that $A_{xz/xy}$ originates from the off-diagonal terms of the Green function $G_{l,m}$ $(l \neq m)$ that is much smaller than the diagonal terms. For this reason, the two-orbiton process is negligible except for $\chi^{\rm TO}_{66}$.

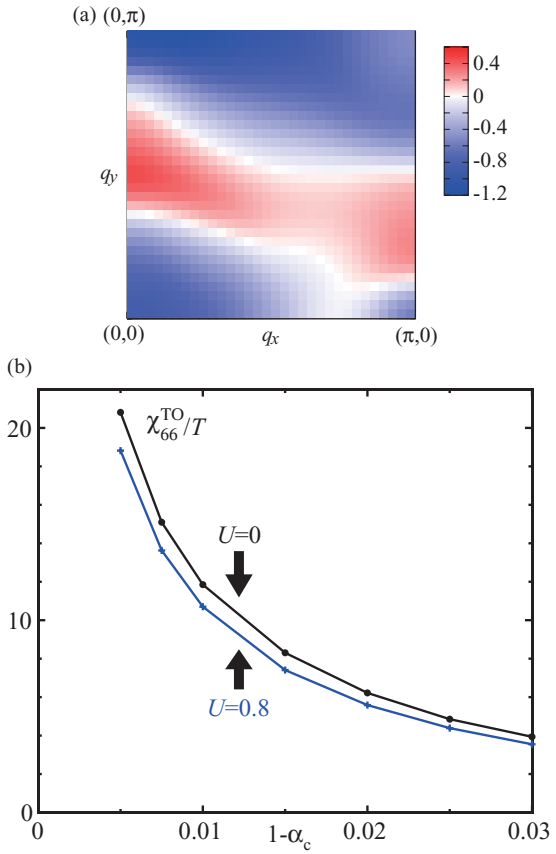

FIG. 9. (Color online) (a) Obtained $A_{x^2-y^2}(xz,xz;\boldsymbol{q})$ for $U=0$. We set $n=6.05$ and $T=0.05$. (b) $\chi^{\rm TO}_{66}/T$ given by Eq. (49) for $U=0$ and 0.8 as a function of α_c. Using the relation $6\xi^2 \sim (1-\alpha_c)^{-1}$ given in the caption of Fig. 4, we obtain $\chi^{\rm TO}_{66}/T \sim 0.1(1-\alpha_c)^{-1} \sim 0.6\xi^2$.

Here, we discuss the softening of C_{66} by taking the two-orbiton process into account: According to Eqs. (39) and (40), we obtain

$$C^{-1}_{66} = C^{-1}_{66,0}[1 + g_{66}\tilde{\chi}_{66}], \quad (51)$$

$$\tilde{\chi}_{66} = \frac{a_{66}+\chi^{\rm TO}_{66}}{1-g_{66}(a_{66}+\chi^{\rm TO}_{66})}, \quad (52)$$

where $a_{66} \equiv 2\chi^0_{66}(\boldsymbol{0},0)$. Now, we consider the case (i) $T_{\rm AFQ} > 0$ and $\omega_0 \ll T$. As we have obtained the relation $\chi^{\rm TO}_{66} \propto T\xi^2$, we set $\chi^{\rm TO}_{66} = b_{66}T/(T-T_{\rm AFQ})$. Since the temperature dependence of a_{66} is small, we obtain

$$\tilde{\chi}_{66} = \frac{a_{66}+b_{66}}{1-g_{66}(a_{66}+b_{66})}\frac{T-[a_{66}/(a_{66}+b_{66})]T_{\rm AFQ}}{T-T_S}, \quad (53)$$

$$T_S = T_{\rm AFQ}\frac{1-g_{66}a_{66}}{1-g_{66}(a_{66}+b_{66})} \ (>T_{\rm AFQ}). \quad (54)$$

Then, the difference between T_S and $T_{\rm AFQ}$, which is conventionally denoted as $E_{\rm JT}$,[51,52] is given by $E_{\rm JT} = T_S(g_{66}b_{66})/(1-g_{66}a_{66}) > 0$. According to Eq. (53), Eq. (51) is rewritten as

$$C_{66} = C_{66,0}[1-g_{66}(a_{66}+b_{66})]\frac{T-T_S}{T-T_{\rm AFQ}}. \quad (55)$$

Here, $g_{66} = 0.1$–0.2 eV and $a_{66} \sim 2\ \mathrm{eV}^{-1}$. We stress that Eqs. (53)–(55) are valid only for $\omega_0 \ll T$.

Finally, we calculate the two-orbiton process analytically for general values of ω_0/T. Since we cannot apply the classical approximation that was used to derive Eq. (49), we have to perform the analytic continuation[57] of Eq. (44). The obtained expression including the quantum fluctuation contribution is given as

$$\chi_{66}^{\mathrm{TO}} = (2g)^4 \{A_{x^2-y^2}(xz,xz;\boldsymbol{Q})\}^2 \sum_{\boldsymbol{q}} \int_{-\infty}^{\infty} \frac{dx}{\pi} n(x) \times 2\,\mathrm{Im}\chi_{xz}^{Q}(\boldsymbol{q},x+i\delta)\,\mathrm{Re}\chi_{xz}^{Q}(\boldsymbol{q},x+i\delta), \tag{56}$$

where $n(x) = (e^{\beta x}-1)^{-1}$ is the Bose distribution function, and we put $A_{x^2-y^2}$ outside of the $\boldsymbol{q}$ summation since its momentum dependence is much smaller than that of χ_{xz}^{Q}. First, we perform the x integration using the following equations:

$$\frac{1}{e^x-1} = \sum_{n=1}^{\infty} \frac{2x}{(2n\pi)^2+x^2} + \frac{1}{x}, \tag{57}$$

$$\int_{-\infty}^{\infty} \frac{x^2}{(a^2+x^2)(b^2+x^2)^2} dx = \frac{\pi}{2b(a+b)^2}, \tag{58}$$

where $a,b>0$. Then, the expression after the x integration in Eq. (56) is given as

$$c^2\xi^4 \left(\omega_0^2 T \sum_{n=1}^{\infty} (B_{\boldsymbol{q}}\omega_0 + 2n\pi T)^{-2} + \frac{T}{2B_{\boldsymbol{q}}^2} \right), \tag{59}$$

where $B_{\boldsymbol{q}} = 1+\xi^2(\boldsymbol{q}-\boldsymbol{Q})^2$. Next, we take the $\boldsymbol{q}$ summation $\sum_{\boldsymbol{q}} \approx \frac{1}{2\pi}\int_0^{\pi} q\,dq$ under the assumption $\xi^2 \gg 1$. Then, the $\boldsymbol{q}$ summation of the second term in Eq. (59) is easily obtained as $c^2\xi^2 T/8$. Also, the $\boldsymbol{q}$-summation of the first term is given as

$$\frac{c^2\xi^2\omega_0}{8\pi} \sum_{n=1}^{n_{\max}} \frac{1}{n+\frac{\omega_0}{2\pi T}} = \frac{c^2\xi^2\omega_0}{8\pi} \left[\psi\left(n_{\max}+\frac{\omega_0}{2\pi T}+1\right) - \psi\left(\frac{\omega_0}{2\pi T}+1\right) \right], \tag{60}$$

where $\psi(x)$ is the di-Gamma function, and the cutoff $n_{\max} \equiv (1+\xi^2\pi^2)\omega_0/2\pi T$ originates from the fact that the $\boldsymbol{q}$ summation is limited to the region $|\boldsymbol{q}| \leqslant \pi$ in periodic systems. As a result, the final expression for the two-orbiton term is

$$\chi_{66}^{\mathrm{TO}} = X\xi^2 \left\{ \frac{\omega_0}{\pi} \left[\psi\left(n_{\max}+\frac{\omega_0}{2\pi T}+1\right) - \psi\left(\frac{\omega_0}{2\pi T}+1\right) \right] + T \right\}, \tag{61}$$

where $X \equiv \frac{(2g)^4c^2}{4\pi}\{A_{x^2-y^2}(xz,xz;\boldsymbol{Q})\}^2$. Here, we verify Eq. (61) in the opposite two limits: In the case (i) $\omega_0 \ll T$, the di-Gamma functions in Eq. (61) are negligible. By applying the relation $\xi^2 = l/(T-T_{\mathrm{AFQ}})$, we obtain

$$\chi_{66}^{\mathrm{TO}} \approx X\xi^2 T \approx b\frac{T}{T-T_{\mathrm{AFQ}}}, \tag{62}$$

where $b = Xl$. The first line in Eq. (62) coincides with Eq. (49) since $\sum_{\boldsymbol{q}}\{\chi_{xz}^{Q}(\boldsymbol{q},0)\}^2 = c^2\xi^2/4\pi$. In the opposite case (ii) $\omega_0 \gg T$, the term T in the curly brackets in Eq. (61) is negligible. Taking the relations $\psi(x) \approx \log(x)$ for $x \gg 1$ and $\omega_0\xi^2 \propto \xi^0$ into account, we obtain

$$\chi_{66}^{\mathrm{TO}} \approx X\xi^2\omega_0 \log(2+\pi^2\xi^2) \approx b'_{66} \log\left(\frac{\pi^2 l}{T-T_{\mathrm{AFQ}}}\right), \tag{63}$$

where $b' = X\xi^2\omega_0$. Therefore, in the case (ii) $T_{\mathrm{AFQ}} < 0$ and $\omega_0 \gg T$, $\tilde{\chi}_{66}$ in Eq. (51) is given by replacing χ_{66}^{TO} with $b'_{66}\log[\pi^2 l/(T-T_{\mathrm{AFQ}})]$ in Eq. (52). In this case, the temperature dependence of χ_{66}^{TO} is quite moderate. In Sec. VI B, we will discuss the temperature dependence of C_{66} based on Eq. (61).

In the above derivation, we have neglected the effect of the mass-enhancement factor brought about by the third point vertex. If we take this effect into account, both Eqs. (62) and (63) are multiplied by the factor $(m^*/m)^2 = 2^2$–3^2, as we will discuss in Sec. VI B.

VI. DISCUSSIONS

A. Why are $O_{x^2-y^2}$-FQ fluctuations the most divergent for $T_{\mathrm{AFQ}} > 0$?

In this paper, we have studied the development of quadrupole susceptibilities in iron pnictides based on the RPA and beyond the RPA. The main fluctuations in the present study are the $O_{xz/yz}$-AFQ fluctuations, $\chi_{xz/yz}^{Q}(\boldsymbol{Q})$, which are produced by Fe-ion in-plane optical phonons. The acoustic phonons $\boldsymbol{q} \sim \boldsymbol{Q}$ with finite energy also assist in producing the AFQ fluctuations; see Eq. (41). We also find that the $O_{x^2-y^2}$-FQ fluctuations, χ_{66}, are induced by the "two-orbiton process" described by the AL-type diagram in Fig. 8(c). Here, the anharmonic three-phonon coupling is produced by the three-point vertex in Eq. (45). The two-orbiton process is important in iron pnictides because of the two-dimensionality.

We discuss the *total susceptibility* by including the electron–acoustic-phonon interaction, $\tilde{\chi}_{\Gamma}^{Q}(\boldsymbol{q})$, by taking the two-orbiton process into account. For $\Gamma = xz$ and x^2-y^2,

$$\tilde{\chi}_{xz}^{Q}(\boldsymbol{Q}) = \frac{\chi_{xz}^{0}(\boldsymbol{Q})}{1-(g+g_{44})\chi_{xz}^{0}(\boldsymbol{Q})}, \tag{64}$$

$$\tilde{\chi}_{x^2-y^2}(\boldsymbol{0}) = \frac{\chi_{66}^{0}(\boldsymbol{0})+\chi_{66}^{\mathrm{TO}}}{1-g_{66}\left[\chi_{66}^{0}(\boldsymbol{0})+\chi_{66}^{\mathrm{TO}}\right]}, \tag{65}$$

where χ_{66}^{TO} is proportional to the square of the AFQ correlation length $\xi^2 \propto \tilde{\chi}_{xz}^{Q}(\boldsymbol{Q})$. When $g_{66} = 0$, therefore, $\tilde{\chi}_{xz}^{Q}(\boldsymbol{Q})$ and $\tilde{\chi}_{x^2-y^2}^{Q}(\boldsymbol{0})$ diverge at the same time in proportion to ξ^2. As g_{66} increases from zero, only $\tilde{\chi}_{x^2-y^2}^{Q}(\boldsymbol{0})$ is enhanced because of the absence of the two-orbiton process; $A_{\Gamma}(xz,xz;\boldsymbol{q}), A_{\Gamma}(yz,yz;\boldsymbol{q}) \ll 1$ for $\Gamma = xz$ or yz as shown in Table I. For this reason, the relation $T_S > T_{\mathrm{AFQ}}$ is universally satisfied even if a fully self-consistent calculation is performed.

As a result, both the AFQ fluctuations (the origin of high-T_c) and the FQ fluctuations (the origin of shear modulus softening) develop at the same time, and latter fluctuations overcome

the former near the T_S. The orthorhombic phase transition in underdoped compounds is caused by the divergence of the two-orbiton process $\tilde{\chi}_{66}$.

B. Softening of C_{66}: Comparison between theory and experiment

Is this subsection, we discuss the softening of C_{66} in under- and overdoped iron pnictides based on the results in Sec. V. For this purpose, we first estimate the magnitude of the three-point vertex $A_{x^2-y^2}(xz,xz,\boldsymbol{Q})$ based on the Ward identity given in Eq. (50). Since $\bar{\chi}^{Q}_{xz,xz}(\boldsymbol{Q},0;0) \sim (2g)^{-1}$, $|A_{x^2-y^2}| \sim (2g)^{-1}/\delta E$, where δE is the bandwidth of the xz/yz band. Since $2g \sim 0.5$ eV and $\delta E \sim 2$ eV according to the band calculations,[2] and considering the effect of band renormalization due to the mass-enhancement factor m^*/m (= 2–3),[58] we expect $|A_{x^2-y^2}| \sim 1(m^*/m)$ (eV^{-2}). This rough estimation is consistent with the numerical result in Fig. 9(a).

Now, we discuss the underdoped case with $T_{\rm AFQ} > 0$. In this case, $\chi^{\rm TO}_{66}/T \approx X\xi^2$ shown in Eq. (62). Using the relations $c \sim 12$ and $6\xi^2 \sim (1-\alpha_c)^{-1}$ as discussed in the caption of Fig. 4, we obtain $X \sim 0.7$ and $\chi^{\rm TO}_{66} \sim 0.12(m^*/m)^2(1-\alpha_c)^{-1}$. This estimation is consistent with the numerical result Fig. 9(b) if we set $(m^*/m) = 1$.

We also discuss the optimum or overdoped systems without structure transition, in which the relation $\omega_0 \gg T$ is satisfied. In this case, $\chi^{\rm TO}_{66} \sim b' \log[\pi^2 l/(T - T_{\rm AFQ})]$. Since the temperature dependence of $\chi^{\rm TO}_{66}$ is moderate, $\chi^{\rm TO}_{66}$ would be comparable to or smaller than a_{66}. Therefore, in overdoped systems, the softening in C_{66} would be quite moderate, showing a deviation from the Curie-Weiss-type form in Eq. (55).

Now, we analyze the temperature dependence of $\chi^{\rm TO}_{66}$ and $C_{66}/C_{66,0}$ by using Eq. (61). We can fix the prefactor $(2g)^4c^2\xi^2\{A_{x^2-y^2}\}^2/4\pi \equiv X\xi^2$ in front of Eq. (61) based on the relation $\chi^{\rm TO}_{66}/T = X\xi^2$ for $\omega_0 \ll T$: We obtain $X \sim 0.6$ according to Fig. 9(b). Hereafter, we set $X = 5.4$ by multiplying the square of the mass-enhancement factor, $(m^*/m)^2 \sim 9$. We also set $\omega_0 = l'(T - T_{\rm AFQ})$ with $l' = 2$, and $\xi^2 = l(T - T_{\rm AFQ})^{-1}$ with $l = 0.086$ (eV), which means that $\xi \sim 2$ when $T - T_{\rm AFQ} = 250$ K. Using the obtained $\chi^{\rm TO}_{66}$, we plot $C_{66}/C_{66,0}$ in Fig. 10(b) based on Eqs. (51) and (52). Here, we set $g_{66} = 0.17$ eV and $a_{66} = 2.5$ eV^{-1}. In the case of $T_{\rm AFQ} = 100$ K, we obtain $E_{\rm JT} \approx 27$ K. In the FLEX approximation,[11] $T_{\rm AFQ}$ changes from positive to negative by carrier doping, while other parameters (X, l, l', and a_{66}) are insensitive to the doping. Similarly to Fig. 10(b), we can fit the recent experimental data by Yoshizawa *et al.*[32] for $Ba(Fe_{1-x}Co_x)_2As_2$ with $x = 0$–0.1 by choosing $T_{\rm AFQ}$ while other parameters (X, l, l', and a_{66}) are fixed. This fact is strong evidence for the success of orbital fluctuation theory in iron pnictide superconductors.

In the present paper, we consider that the origin of high-T_c is the AFQ fluctuations. On the other hand, Yanagi *et al.*[43] claimed that high-T_c originates from the FQ fluctuations that give the softening in C_{66}: In the latter mechanism, a rough estimation of T_c is given as

$$T_c \sim \omega_c \exp[-(1+\beta\lambda)/\beta\lambda], \qquad (66)$$

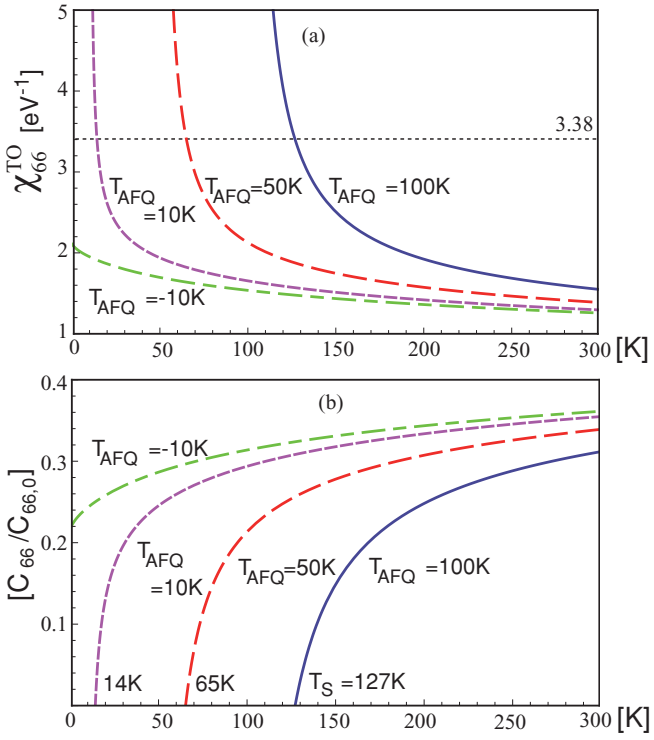

FIG. 10. (Color online) (a) $\chi^{\rm TO}_{66}$ for $T_{\rm AFQ} = 100$, 50, 10, and -10 K given by Eq. (61). (b) $C_{66}/C_{66,0}$ for $T_{\rm AFQ} = 100$, 50, 10, and -10 K given by Eqs. (51) and (52). We set $X = 5.7$, $l = 0.086$, $l' = 2$, $g_{66} = 0.17$, and $a_{66} = 2.5$. $C_{66} = 0$ is realized when $\chi^{\rm TO}_{66} = g^{-1}_{66} - a_{66}$, which is 3.38 in the present parameters. Using these *same* parameters, we can fit the recent experimental data by Yoshizawa *et al.*[32] for $Ba(Fe_{1-x}Co_x)_2As_2$ for $x = 0$–0.1 just by changing $T_{\rm AFQ}$.

where ω_c is the phonon energy relevant for the orbital fluctuations, which is just $\sim$10 K for $|\boldsymbol{q}| \sim 0.1\pi$. $\beta \equiv 1 + g_{66}\tilde{\chi}_{66} = C_{66,0}/C_{66}$ is the enhancement factor due to FQ fluctuations.[44] However, $C_{66,0}/C_{66}$ observed in optimally doped $Ba(Fe,Co)_2As_2$ is just $\sim$1.2:[30,32] Apparently, such a small enhancement cannot reproduce high-T_c superconductivity in iron pnictides.

In the present study, in contrast, weak softening in optimally doped samples is ascribed to the change in the scaling of $\chi^{\rm TO}_{66}$, not to the weakness of AFQ fluctuations. In fact, the softening is moderate in the case of $T_{\rm AFQ} = -10$ K in Fig. 10, while the AFQ correlation $\xi^2 \approx 1000/[T\ ({\rm K}) + 10]$ is enough to cause the superconductivity at $T_c \sim 30$ K. Therefore, moderate softening and high-T_c are compatible in the present study.

C. Quadrupole-ordered state in underdoped compounds

Here, we consider the orbital or quadrupole ordered state in underdoped compounds. In the mean-field approximation for the multi-orbital Hubbard model for iron pnictides,[59,60] stripe-type SDW order occurs for $U > U_c$, and weak orbital polarization ($n_{xz} \neq n_{yz}$) is induced as the secondary order when the magnetization is large. However, in real materials, orthorhombic transition occurs in the paramagnetic state, and the SDW order is induced in the orthorhombic phase. To solve this problem, we studied the multi-orbital HH model beyond the mean-field theory, and found that the FQ order occurs in the paramagnetic state due to the two-orbiton process. Fortunately,

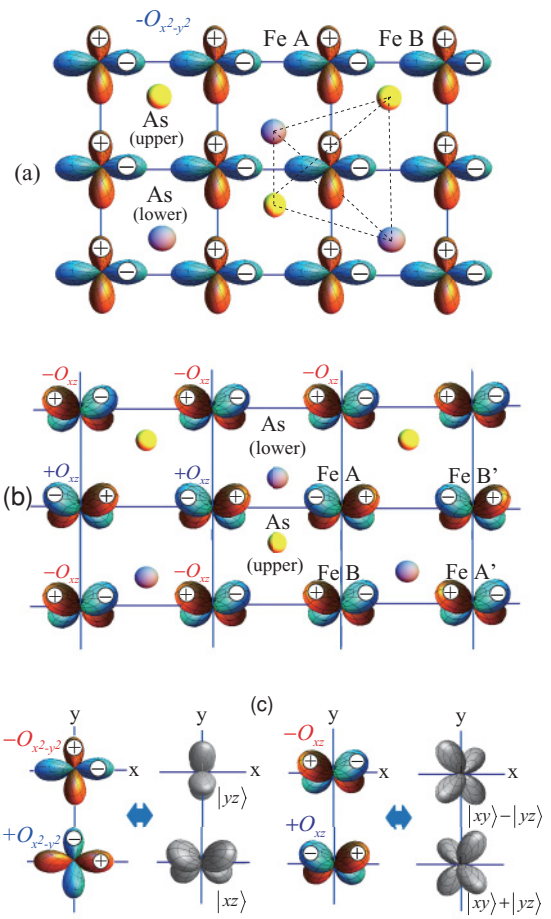

FIG. 11. (Color online) (a) $O_{x^2-y^2}$-FQ order given by the divergence of C_{66}^{-1}. Be careful not to confuse $\hat{O}_{x^2-y^2}$ with the (x^2-y^2)-orbital operator. (b) O_{xz}-AFQ order brought by the divergence of $\chi^{Q}_{xz}(\boldsymbol{Q})$. (c) The correspondence between $O_{x^2-y^2}$-quadrupole order (O_{xz}-quadrupole order) and the d orbital with larger occupation number.

this FQ order does produce the experimentally observed SDW order, as we will explain in the next subsection.

As discussed in Sec. V B, the divergence of $\tilde{\chi}_{66}$, which is the total FQ susceptibility given by both optical and acoustic phonons, causes the orthorhombic structure transition when $C_{66}=0$. The $O_{x^2-y^2}$-FQ order is realized in the orthorhombic phase. The schematic quadrupole order is shown in Fig. 11(a). Since $O_{x^2-y^2}\approx n_2-n_3$ according to Eq. (7), the order parameter $O_{x^2-y^2}>0$ (<0) corresponds the orbital polarized state with $n_{xz}>n_{yz}$ ($n_{xz}<n_{yz}$). Figure 11(b) shows the AFQ order brought about by the divergence of $\chi^{Q}_{xz}(\boldsymbol{Q})$. Although the FQ order in (a) would occur earlier, we expect the AFQ order in (b) would coexist with the FQ order when the structure transition is the weak first order. In fact, the reconstruction of the FS's above $T_{\rm N}$ in detwinned $Ba(Fe_{1-x}Co_x)_2As_2$ (Ref. 25) would indicate the presence of the AFQ order.[61]

In Fig. 11(c), we show the correspondence between the quadrupole order and the d-wave function with larger electron occupancy. In the $O_{x^2-y^2}$-type quadrupole order, the electrons mainly occupy the state $|xz\rangle$ for $O_{x^2-y^2}>0$, or the state $|yz\rangle$ for $O_{x^2-y^2}<0$. In the O_{xz}-type quadrupole order, the electrons mainly occupy the state $|xy\rangle+|xz\rangle$ for $O_{xz}>0$ ($|xy\rangle-|xz\rangle$ for $O_{xz}<0$).

Finally, we make a comparison between the present study and the previous work based on the RPA,[43] which claims that the divergence of Eq. (51) is caused by large $g_{66}a_{66}\lesssim 1$ while neglecting $\chi^{\rm TO}_{66}$. However, the obtained $O_{x^2-y^2}$-quadrupole order is "incommensurate."[46] This result highlights the importance of the two-orbiton process $\chi^{\rm TO}_{66}$ to produce the "$\boldsymbol{q}=0$" orthorhombic structure transition.

D. Stripe magnetic order produced by $O_{x^2-y^2}$-FQ order

In underdoped iron pnictides, the collinear-SDW order is induced in the orthorhombic phase at $T_{\rm N}$, which is slightly lower temperature than T_S. Various explanations for the origin of this SDW transition have been proposed previously. From a strong-coupling scheme, the square-lattice Heisenberg model with in-plane anisotropy, the J_{1a}-J_{1b}-J_2 model, has been studied.[26] According to the neutron scattering on $CaFe_2As_2$,[34] the high-energy spin-wave dispersion indicates the relation $J_{1a}\gg J_{1b}$ in the orthorhombic phase. In this case, experimentally observed staggered spin order along the x axis (a axis) is expected to be realized. However, such strong in-plane anisotropy $J_{1a}\gg J_{1b}$ is surprising, considering the small orthorhombicity $(a-b)/(a+b)\sim 0.003$. These facts indicate the existence of orbital or quadrupole order in the orthorhombic phase.

In this subsection, we study the origin of the SDW state based on the weak-coupling approach. Hereafter, we assume that the x axis corresponds to the a axis (longer lattice constant) in the orthorhombic phase. In the previous subsection, we explained that the two-orbital process induces the $O_{x^2-y^2}$-FQ order in Fig. 11. Note that $O_{x^2-y^2}\approx n_2-n_3$ according to Eq. (7). The corresponding mean field is given as

$$H'=\Delta E\sum_i (|2\rangle\langle 2|-|3\rangle\langle 3|)_i\,, \tag{67}$$

which raises (lowers) the energy level of orbital 2 (3) by ΔE. In a similar model, the change in the DOS and FS's by the orthorhombic potential ΔE was studied by Chen *et al.*[62] Here, we study the change in the spin susceptibility by ΔE using the RPA.

We calculate the total spin susceptibility $\chi^s(\boldsymbol{q},0)=\sum_{l,m}\chi^s_{l,l;m,m}(\boldsymbol{q},0)$ for $U=1.1$ and $g=0$. Figure 12(a) shows the obtained $\chi^s(\boldsymbol{q},0)$ for $\Delta E=0$; the corresponding spin Stoner factor is $\alpha_S=0.87$. When ΔE is finite, the four-hold symmetry in $\chi^s(\boldsymbol{q},0)$ disappears quickly. Figure 12(b) shows the change in the spin susceptibility, $\chi^s(\boldsymbol{q};\Delta E)-\chi^s(\boldsymbol{q};0)$, induced by $\Delta E=+0.04$. We see that $\chi^s(\boldsymbol{q},0)$ increases by $+6.5$ at $\boldsymbol{q}=(0,\pi)$ while it decreases by -4.0 at $\boldsymbol{q}=(\pi,0)$. Therefore, magnetic frustration is resolved and stripe-SDW order can be induced by small ΔE.

Figure 12(c) shows the ΔE-U_c phase diagram given by the RPA, that is, by the mean-field approximation. It is noteworthy that U_c quickly decreases in proportion to $|\Delta E|$ because of the degeneracy of orbitals 2 and 3. When $U\lesssim U_c$, the experimental SDW order with momentum $\boldsymbol{q}=(\pi,0)$ is realized by the negative potential ΔE that corresponds to $n_2>n_3$. Figure 12(d) displays the relation between $\Delta n=\Delta n_2-\Delta n_3$ and ΔE: If we take the band-renormalization effect into account, we obtain the relation $\Delta n=-0.85(m^*/m)\Delta E$.

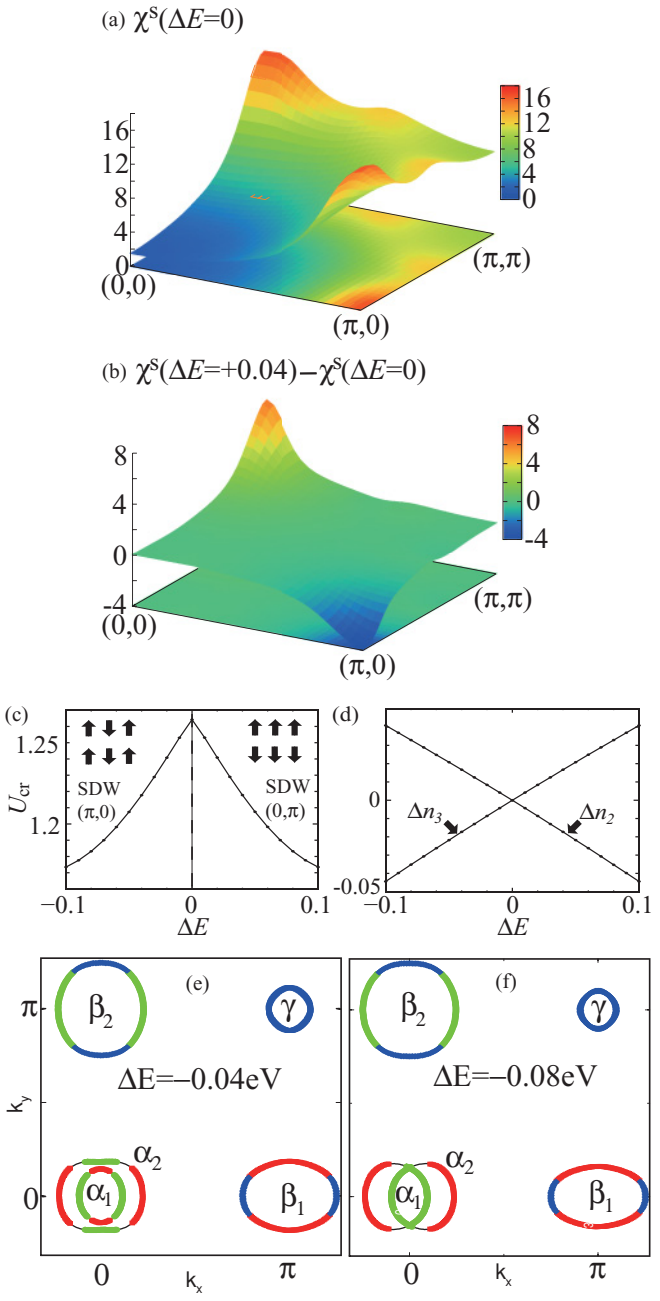

FIG. 12. (Color online) (a) $\chi^s(\boldsymbol{q};\Delta E)$ for $\Delta E = 0$. Used model parameters are $n = 6.05$, $U = 1.1$, $g = 0$, and $T = 0.05$. (b) $\chi^s(\boldsymbol{q};\Delta E) - \chi^s(\boldsymbol{q};0)$ for $\Delta E = 0.04$. Model parameters are the same as those in (a). (c) U_c as a function of ΔE given by the RPA for $m^*/m = 1$. (d) Δn_2 and Δn_3 as a function of ΔE for $m^*/m = 1$. Note that $\Delta n \equiv \Delta n_2 - \Delta n_3$. (e) FS's for $\Delta E = -0.04$ for $n = 6.05$. We use the same color coding as in Fig. 2. (f) FS's for $\Delta E = -0.08$ for $n = 6.05$. In both cases, the best nesting vector is $\boldsymbol{q} = (\pi,0)$.

According to (c) and (d), we obtain the reduction in U_c due to the FQ order as

$$\Delta U_c = -1.4|\Delta n| = -1.2(m^*/m)|\Delta E|. \tag{68}$$

Therefore, only a few percent of Δn can induce a large change in U_c that is *linear in* $|\Delta n|$. According to recent ARPES measurement in detwinned $BaFe_2As_2$,[25] $\Delta E \sim -0.03$ eV in the orthorhombic phase, which corresponds to $\Delta n = +0.026(m^*/m)$ and $\Delta U_c = -0.036(m^*/m)$ in the present five-orbital model. In this case, the realized SDW order is $\boldsymbol{q} = (\pi,0)$, which is consistent with the famous stripe-type SDW state in mother compounds.[22]

We can show that the SDW temperature T_N also increases *linearly in* $|\Delta n|$ based on the Landau theory. The free energy in the present problem would be given as

$$F(\Delta n) = F(0) + c\Delta n\left(m^2_{(\pi,0)} - m^2_{(0,\pi)}\right), \tag{69}$$

where $m_{\boldsymbol{Q}}$ is the AF order with momentum $\boldsymbol{Q}$, and $F(0) = a(T - T_N^0)(m^2_{(\pi,0)} + m^2_{(0,\pi)}) + b(m^4_{(\pi,0)} + m^4_{(0,\pi)})/2 + \cdots$ with $a,b > 0$. Then, we obtain $T_N = T_N^0 + |c\Delta n|/a$. The present study shows that $c < 0$, which seems consistent with the numerical result in Ref. 60.

Now, we consider the reason why SDW order is produced by ΔE. Figures 12(e) and 12(f) show the change in the the FS structure with ΔE. We can recognize that the intra-orbital (orbital 3) nesting between FS α_2 and FS β_1 becomes better, compared to the case of $\Delta E = 0$ in Fig. 2(a). Therefore, the origin of the "FQ-order-induced stripe SDW" is the "anisotropy in the intra-orbital nesting" caused by small $|\Delta E| \sim 0.03$ eV, which corresponds to a small orbital polarization $|\Delta n| \sim 0.026(m^*/m)$. This result is consistent with the very small orthorhombicity $(a-b)/(a+b) \lesssim 0.003$ in the orthorhombic state.[22] In the strong-coupling description, the origin of the stripe-SDW state is the in-plane anisotropy in the exchange interaction ($J_{1a} \neq J_{1b}$)[26,34] brought by two-orbiton process.

If we go beyond the RPA, the SDW state will be further stabilized by the reduction in the quasiparticle damping γ when the FQ order is established:[11] In fact, in the FLEX approximation,[11] $\chi^s(\boldsymbol{q})$ is suppressed by γ due to strong orbital fluctuations in the normal state. Since the orbital fluctuations are suppressed when the AFQ order sets in, the resulting increment in $\chi^s(\boldsymbol{q})$ would stabilize the SDW phase.

E. Summary

In the present paper, we have studied the realistic five-orbital HH model for iron pnictides. In the RPA, only the O_{xz}-AFQ fluctuations develop as shown previously,[9] and therefore the softening of shear moduli (C_{66}, C_{44}, and C_E) cannot be reproduced. In the present study beyond the RPA, we revealed that both O_{xz}-AFQ fluctuations and $O_{x^2-y^2}$-FQ fluctuations develop at the same time. The former and the latter fluctuations are the origins of the s_{++}-wave superconductivity and the orthorhombic structure transition, respectively. The commensurate FQ fluctuations are brought about by the two-orbiton process in Fig. 8(c) that is dropped in the RPA. (In the mean-field theory, the orbital order due to large g_{66} is always "incommensurate.")[46] Fluctuation-induced softening occurs only in C_{66} out of three shear moduli because of the orbital selection rule for the three-point vertex. The origin of softening would be interpreted as "virtual anharmonicity of lattice vibrations" that is induced by AFQ fluctuations; see Fig. 8(b). Possible quadrupole orders in the ordered state are shown in Fig. 11. Using the two-orbiton term in Eq. (61), we can fit the recent experimental data of C_{66} in $Ba(Fe_{1-x}Co_x)_2As_2$ (Ref. 32) for a wide range of doping, only by choosing T_{AFQ} while other parameters are fixed. This fact is strong evidence

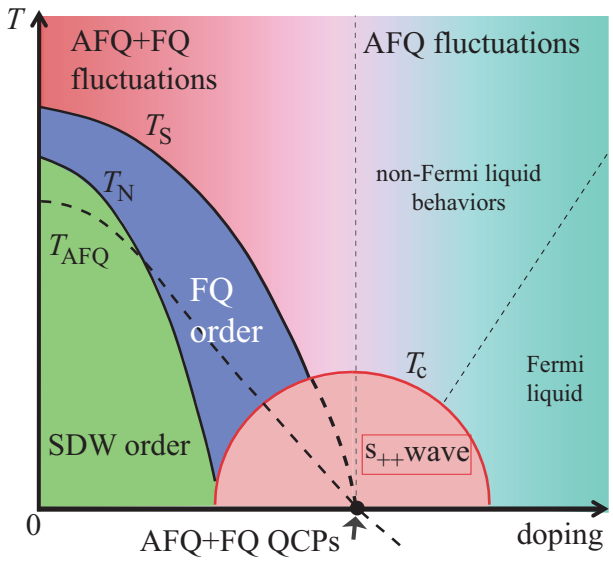

FIG. 13. (Color online) The phase diagram for iron-pnictide superconductors obtained by the present orbital fluctuation theory. T_S is the orthorhombic transition temperature (= FQ order temperature), and T_N is the SDW transition temperature. The fact that two QCP's at $T_S = 0$ and $T_{AFQ} = 0$ almost coincide means that novel "multi-orbital QCP's" are realized in iron pnictides. The left-hand (right-hand) side of the vertical dotted line corresponds to $T_{AFQ} > 0$ ($T_{AFQ} < 0$), in which the two-orbiton process is relevant (irrelevant). At T_{AFQ}, the AFQ order does not occur since it is prevented by the FQ order at T_S.

for the success of orbital fluctuation theory in iron pnictide superconductors.

In addition, we should stress that the stripe-type antiferromagnetic state is realized in the orbital-ordered state, since the small orbital polarization ($\Delta n \lesssim 0.05$) can cause large in-plane anisotropy in the exchange interaction ($J_{1a} \neq J_{1b}$). Thus, the present study presents a microscopic justification for the anisotropic Heisenberg model description for the SDW state.[26,34]

In Fig. 13, we summarize the phase diagram of iron pnictides given by the present orbital fluctuation theory beyond the RPA. We stress that T_{AFQ}, which is determined experimentally from C_{66}, is positive in the underdoped case ($T_S > 0$) while it is negative in the overdoped case, as recognized from Eq. (54) obtained in the classical approximation. In particular, $T_S \approx 0$ for $T_{AFQ} = 0$, consistently with experiments.[31,33] This result indicates that QCP's for AFQ and FQ orders almost coincide at the end point of the orthorhombic phase. The emergence of "multi-orbital QCP's" is favorable to the orbital-fluctuation-mediated s_{++}-wave SC state.[9–11] In fact, T_{AFQ} is derived from experimentally observed C_{66} as follows: In under-doped systems with $T_S > 0$, T_{AFQ} is given the Weiss temperature of $C_{66} \propto (T - T_S)/(T - \theta)$, and $T_{AFQ} = \theta$ is indeed positive experimentally. In over-doped systems, both T_S and θ are negative ($T_S > \theta$), and C_{66} starts to deviate from the Curie-Weiss behavior. These experimental results are the strong evidence for the realization of the two-orbiton process ($\sim T/(T - T_{AFQ})$) in iron pnictides. In contrast, in the cooperative Jahn-Teller scenario due to large g_{66} by Yanagi *et al.*,[43] the parameter θ is always negative; see Appendix A in detail.

In summary, the present study can explain the superconductivity, orthorhombic transition, and softening of C_{66} due to FQ and AFQ quantum criticalities. The stripe-SDW order is naturally produced by the "orthorhombicity" of the FQ order. These results are strong evidence for the realization of the orbital-fluctuation-mediated s_{++}-wave superconductivity in iron pnictides. Finally, we stress that the present study enables us to derive the important parameters in the orbital fluctuation model in Eqs. (46)–(48) from the experimental data of shear modulus.

ACKNOWLEDGMENTS

We are grateful to M. Yoshizawa for valuable discussions on his interesting experimental results. We also thank D. S. Hirashima, M. Sato, Y. Matsuda, and T. Shibauchi for valuable comments and discussions. This study has been supported by Grants-in-Aid for Scientific Research from MEXT of Japan, and by JST, TRIP. Numerical calculations were performed using the facilities of the supercomputer center, Institute for Molecular Science.

APPENDIX A: STRUCTURE TRANSITIONS IN ITINERANT ELECTRON SYSTEMS: QUADRUPOLE-QUADRUPOLE INTERACTION VERSUS COOPERATIVE JAHN-TELLER EFFECT

In this paper, we studied the structure transition due to $O_{x^2-y^2}$-FQ order in iron-pnictides. The ferroquadrupole interaction originates from the two-orbiton process with respect to O_{xz}-AFQ fluctuations, which are induced by optical phonons. The $O_{x^2-y^2}$-FQ fluctuations give the softening of the elastic constant C_{66}.

In this Appendix, we present a general theory for the structure transitions in itinerant metals, and we consider the uniqueness of iron pnictides in the next step. The structure transition due to ferroquadrupole order is classified as the "cooperative Jahn-Teller type" or "quadrupole-quadrupole interaction type."[52] The elastic constant C_ϕ is given by Eqs. (39) and (40), where χ_ϕ is the quadrupole susceptibility at $\boldsymbol{q} = 0$ without acoustic phonons. Now, we introduce the quadrupole-quadrupole interaction g like in Eq. (10), the origin of which is the optical phonons or Coulomb interaction. In the RPA, $\chi_\phi = \chi_\phi^0/(1 - g\chi_\phi^0)$, where χ_ϕ^0 is the bare quadrupole susceptibility. Then, C_ϕ is given as

$$\frac{C_\phi}{C_{\phi,0}} = \frac{1 - (g_{ac} + g)\chi_\phi^0}{1 - g\chi_\phi^0}. \tag{A1}$$

In rare-earth metals in which f electrons are localized, χ_ϕ^0 is proportional to $1/T$.[51,52] However, this replacement is inappropriate in itinerant metals. In nearly ferroquadrupole itinerant metals, $|1 - (g_{ac} + g)\chi_\phi^0| \ll 1$ at zero temperature.

Here, we consider the temperature dependence of C_ϕ beyond the RPA. In the FLEX approximation[11] or SCR theory,[56] χ_ϕ^0 is replaced with $\chi_\phi^0 - \alpha T$ ($\alpha > 0$) due to the thermal fluctuations, which are mainly described as the self-energy. In this case, Eq. (A1) becomes

$$\frac{C_\phi}{C_{\phi,0}} \approx \frac{T - T_S}{T - \theta}, \tag{A2}$$

where $T_S = -[1-(g_{\rm ac}+g)\chi_\phi^0]/(g_{\rm ac}+g)\alpha$ and $\theta = -(1-g\chi_\phi^0)/g\alpha$. Therefore, C_ϕ shows the Curie-Weiss behavior in the RPA by taking the thermal fluctuations into account.

First, we consider the case (i) $g_{\rm ac} \ll g$, in which the structure transition is driven by quadrupole-quadrupole interaction.[52] In this case, $E_{\rm JT} \equiv T_S - \theta \approx g_{\rm ac}/g^2\alpha$, which is much smaller than T_S. (Note that C_ϕ does not soften when $g_{\rm ac} = 0$.) Then, the lattice distortion in the ordered state will be very small ($\ll 1\%$), as in $PrRu_4P_{12}$. In the opposite case (ii) $g_{\rm ac} \gg g$, the structure transition is driven by the cooperative Jahn-Teller effect.[52] In this case, $\theta \approx -1/g\alpha$, which takes a large negative value since α is small; $\theta \sim -300$ K. Then, the lattice distortion in the ordered state should be very large ($\gg 1\%$), like manganites. In case (ii), the energy of the "ferro-orbital fluctuations" induced by the acoustic phonon is very low, and the T_c of the orbital-fluctuation superconductivity is still lower. Therefore, the emergence of high-T_c superconductivity is unlikely in case (ii).

In the case of C_{66} in iron pnictides, quadrupole-quadrupole interaction g due to optical phonons is absent. Moreover, $O_{x^2-y^2}$-FQ fluctuations due to Coulomb interaction do not develop even in the $U' > U$ model.[41] Therefore, if we try to explain the C_{66} softening within the RPA, we have to assume the case (ii), i.e., the cooperative Jahn-Teller transition as proposed by Yanagi *et al.*[43] However, it contradicts with experiments facts, that is, $(a-b)/(a+b) \lesssim 0.3\%$ and $n_{xz} - n_{yz} \lesssim 5\%$ in the orthorhombic phase irrespective of higher T_S ($\sim$100 K), and $\theta > 0$ in the underdoped pnictides. Therefore, the RPA analysis done by Yanagi *et al.*[43] is inconsistent with experiments.

In this paper, we studied the structure transition in case (i), i.e., the quadrupole-quadrupole interaction type. The origin of quadrupole-quadrupole interaction is the "two-orbiton process," which is not taken into account in the RPA. In two-dimensional systems, the two-orbiton process gives the Curie-Weiss behavior in Eq. (A2), if allowed by the orbital selection rule discussed in Sec. VI B. By using reasonable sets of parameters ($g_{\rm ac} < g$), experimentally observed Curie-Weiss behavior of C_{66} in underdoped pnictides ($T_S > 0$)[31,33] is well reproduced, given in Eq. (55): According to Eq. (54), $T_{\rm AFQ}$ ($= \theta$) is positive in underdoped pnictides and $T_{\rm AFQ} \approx 0$ at the critical point $T_S = 0$, consistent with experimental reports.[33] In overdoped pnictides, the softening of C_{66} becomes moderate since the two-orbiton process gives a very weak temperature dependence.

APPENDIX B: QUADRUPOLE SUSCEPTIBILITIES IN THE TEN-ORBITAL MODEL: EFFECT OF UNFOLD GAUGE TRANSFORMATION

In Sec. III, we calculated $\chi_\Gamma^Q(\boldsymbol{q},0)$ based on the five-orbital model using the RPA, shown in Fig. 4. In this Appendix, we discuss the effect of the unfold gauge transformation in deriving the five-orbital model on $\chi_\Gamma^Q(\boldsymbol{q},0)$. This gauge transition changes the signs of (2,3) orbitals for Fe-B sites. Therefore, signs of quadrupole operators $\hat{O}^i_{xz/yz}$ at Fe-B sites are reversed, as recognized in Eqs. (4)–(8). For this reason, $\chi^Q_{xz,yz}(\boldsymbol{q},\omega)$ is not gauge-invariant since it contains linear terms with respect to $\hat{O}^i_{xz/yz}$, although the el-el interaction in Eqs. (14)–(16) is gauge invariant.

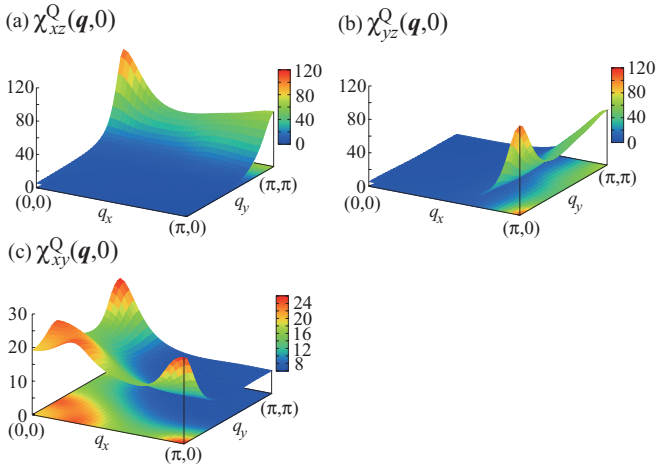

FIG. 14. (Color online) Quadrupole susceptibilities in the ten-orbital model for (a) $\chi^Q_{xz}(\boldsymbol{q})$, (b) $\chi^Q_{yz}(\boldsymbol{q})$, and (c) $\chi^Q_{xy}(\boldsymbol{q})$, respectively. We set $n = 6.05$, $T = 0.05$, and $\alpha_c = 0.98$.

From now on, we calculate the quadrupole susceptibilities in the ten-orbital model. We describe the orbitals of Fe-A (Fe-B) ions as $1 \sim 5$ ($6 \sim 10$). In the RPA, the susceptibilities are given as

$$\chi^Q_\Gamma(q) = \chi^{Q,AA}_\Gamma(q) + \chi^{Q,AB}_\Gamma(q), \tag{B1}$$

$$\chi^{Q,AA(AB)}_\Gamma(q) = \sum_{ll'}^{A}\sum_{mm'}^{A(B)} o^{ll'}_\Gamma \chi^c_{ll'mm'}(q) o^{mm'}_\Gamma \tag{B2}$$

for $\Gamma = xz, yz, xy$, where $o^{lm}_\Gamma = o^{l-5,m-5}_\Gamma$ for $l,m \geqslant 6$. The obtained quadrupole susceptibilities in Eq. (B1) is show in

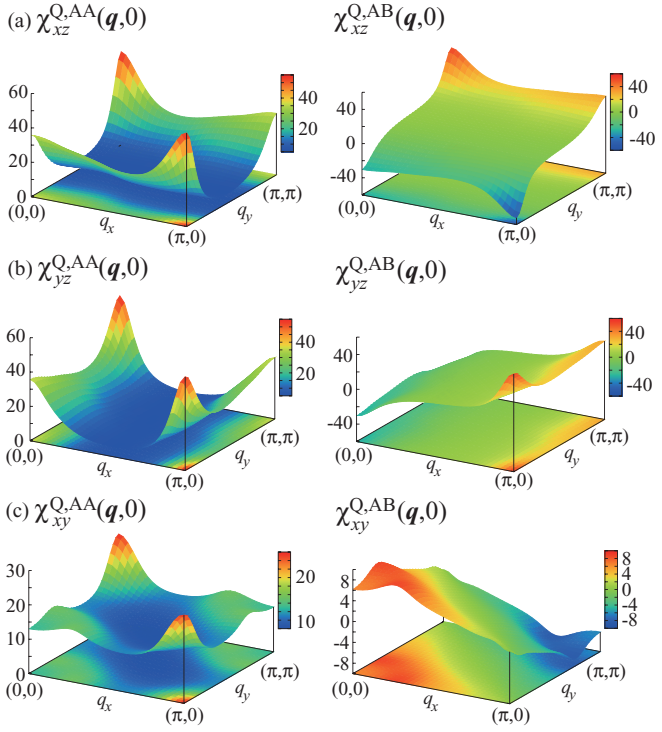

FIG. 15. (Color online) Quadrupole susceptibilities in the ten-orbital model for (a) $\chi^{Q,AA}_{xz}(\boldsymbol{q})$ and $\chi^{Q,AB}_{xz}(\boldsymbol{q})$, (b) $\chi^{Q,AA}_{yz}(\boldsymbol{q})$ and $\chi^{Q,AB}_{yz}(\boldsymbol{q})$, and (c) $\chi^{Q,AA}_{xy}(\boldsymbol{q})$ and $\chi^{Q,AB}_{xy}(\boldsymbol{q})$, respectively. We set $n = 6.05$, $T = 0.05$, and $\alpha_c = 0.98$.

Fig. 14, and its diagonal and off-diagonal terms with respect to A and B are also shown in Fig. 15. In these figures, we have unfolded the susceptibilities into the single-iron BZ to make a comparison with Fig. 4. According to Eq. (B1), $\chi_{\Gamma}^{Q}(q)$ in the ten-orbital model is given by $\chi_{\Gamma}^{Q,AA}(q)+\chi_{\Gamma}^{Q,AB}(q)$. We see that $\chi_{xz}^{Q}(\boldsymbol{q},0)$ is Fig. 14(a) has a sharp peak at $\boldsymbol{q}=(0,\pi)$, since both $\chi_{xz}^{Q,AA}(q)$ and $\chi_{xz}^{Q,AB}(q)$ in Fig. 15(a) have peaks at $\boldsymbol{q}=(0,\pi)$.

If we perform the unfold gauge transformation, the sign of $\chi_{\Gamma}^{Q,AB}(q)$ is inverted for $\Gamma=xz$ and yz. Therefore, in the five-orbital model, $\chi_{\Gamma}^{Q}(q,0)=\chi_{\Gamma}^{Q,AA}(q)-\chi_{\Gamma}^{Q,AB}(q)$ for $\Gamma=xz$ and yz. For this reason, the peak in $\chi_{xz}^{Q}(\boldsymbol{q},0)$ moves from $\boldsymbol{q}=(0,\pi)$ to $(\pi,0)$ under the gauge transformation, consistently with the result in Fig. 4(a). In contrast to $\chi_{xz/yz}^{Q,AB}(\boldsymbol{q})$, $\chi_{xy}^{Q}(\boldsymbol{q})$ is gauge invariant. For this reason, Fig. 14(c) in the ten-orbital model coincides with Fig. 4(c) in the five-orbital model.

[1] Y. Kamihara, T. Watanabe, M. Hirano, and H. Hosono, J. Am. Chem. Soc. **130**, 3296 (2008).

[2] K. Kuroki, S. Onari, R. Arita, H. Usui, Y. Tanaka, H. Kontani, and H. Aoki, Phys. Rev. Lett. **101**, 087004 (2008).

[3] I. I. Mazin, D. J. Singh, M. D. Johannes, and M. H. Du, Phys. Rev. Lett. **101**, 057003 (2008).

[4] S. Graser, G. R. Boyd, C. Cao, H.-P. Cheng, P. J. Hirschfeld, and D. J. Scalapino, Phys. Rev. B **77**, 180514(R) (2008).

[5] A. V. Chubukov, D. V. Efremov, and I. Eremin, Phys. Rev. B **78**, 134512 (2008).

[6] S. Onari and H. Kontani, Phys. Rev. Lett. **103**, 177001 (2009).

[7] A. Kawabata, S. C. Lee, T. Moyoshi, Y. Kobayashi, and M. Sato, J. Phys. Soc. Jpn. Suppl. C **77**, 103704 (2008); M. Sato, Y. Kobayashi, S. C. Lee, H. Takahashi, E. Satomi, and Y. Miura, J. Phys. Soc. Jpn. **79**, 014710 (2009); S. C. Lee, E. Satomi, Y. Kobayashi, and M. Sato, *ibid.* **79**, 023702 (2010).

[8] Y. Nakajima, T. Taen, Y. Tsuchiya, T. Tamegai, H. Kitamura, and T. Murakami, Phys. Rev. B **82**, 220504 (2010).

[9] H. Kontani and S. Onari, Phys. Rev. Lett. **104**, 157001 (2010).

[10] T. Saito, S. Onari, and H. Kontani, Phys. Rev. B **82**, 144510 (2010).

[11] S. Onari and H. Kontani, e-print arXiv:1009.3882.

[12] C.-H. Lee, A. Iyo, H. Eisaki, H. Kito, M. T. Fernandez-Diaz, T. Ito, K. Kihou, H. Matsuhata, M. Braden, and K. Yamada, J. Phys. Soc. Jpn. **77**, 083704 (2008).

[13] T. Shimojima, F. Sakaguchi, K. Ishizaka, Y. Ishida, T. Kiss, M. Okawa, T. Togashi, C.-T. Chen, S. Watanabe, M. Arita, K. Shimada, H. Namatame, M. Taniguchi, K. Ohgushi, S. Kasahara, T. Terashima, T. Shibauchi, Y. Matsuda, A. Chainani, and S. Shin, Science **332**, 564 (2011).

[14] A. D. Christianson, E. A. Goremychkin, R. Osborn, S. Rosenkranz, M. D. Lumsden, C. D. Malliakas, I. S. Todorov, H. Claus, D. Y. Chung, M. G. Kanatzidis, R. I. Bewley, and T. Guidi, Nature (London) **456**, 930 (2008); Y. Qiu, W. Bao, Y. Zhao, C. Broholm, V. Stanev, Z. Tesanovic, Y. C. Gasparovic, S. Chang, J. Hu, B. Qian, M. Fang, and Z. Mao, Phys. Rev. Lett. **103**, 067008 (2009); D. S. Inosov, J. T. Park, P. Bourges, D. L. Sun, Y. Sidis, A. Schneidewind, K. Hradil, D. Haug, C. T. Lin, B. Keimer, and V. Hinkov, Nat. Phys. **6**, 178 (2010).

[15] T. A. Maier and D. J. Scalapino, Phys. Rev. B **78**, 020514(R) (2008); T. A. Maier, S. Graser, D. J. Scalapino, and P. J. Hirschfeld, Phys. Rev. B **79**, 224510 (2009).

[16] M. M. Korshunov and I. Eremin, Phys. Rev. B **78**, 140509(R) (2008).

[17] S. Onari, H. Kontani, and M. Sato, Phys. Rev. B **81**, 060504(R) (2010)

[18] M. Sato *et al.* (private communications).

[19] T. A. Maier, S. Graser, P. J. Hirschfeld, and D. J. Scalapino, Phys. Rev. B **83**, 220505(R) (2011).

[20] S. Kasahara, T. Shibauchi, K. Hashimoto, K. Ikada, S. Tonegawa, R. Okazaki, H. Shishido, H. Ikeda, H. Takeya, K. Hirata, T. Terashima, and Y. Matsuda, Phys. Rev. B **81**, 184519 (2010).

[21] H. Kontani, Rep. Prog. Phys. **71**, 026501 (2008); H. Kontani and K. Yamada, J. Phys. Soc. Jpn. **74**, 155 (2005); H. Kontani, K. Kanki, and K. Ueda, Phys. Rev. B **59**, 14723 (1999).

[22] D. C. Jhonston, Adv. Phys. **59**, 803 (2010).

[23] T. Shimojima, K. Ishizaka, Y. Ishida, N. Katayama, K. Ohgushi, T. Kiss, M. Okawa, T. Togashi, X.-Y. Wang, C.-T. Chen, S. Watanabe, R. Kadota, T. Oguchi, A. Chainani, and S. Shin, Phys. Rev. Lett. **104**, 057002 (2010).

[24] Q. Wang, Z. Sun, E. Rotenberg, F. Ronning, E. D. Bauer, H. Lin, R. S. Markiewicz, M. Lindroos, B. Barbiellini, A. Bansil, and D. S. Dessau, e-print arXiv:1009.0271.

[25] M. Yi, D. H. Lu, J.-H. Chu, J. G. Analytis, A. P. Sorini, A. F. Kemper, S.-K. Mo, R. G. Moore, M. Hashimoto, W. S. Lee, Z. Hussain, T. P. Devereaux, I. R. Fisher, and Z.-X. Shen, Proc. Natl. Acad. Sci. USA **108**, 6878 (2011).

[26] T. Yildirim, Physica C **469**, 425 (2009); F. Kruger, S. Kumar, J. Zaanen, and J. van den Brink, Phys. Rev. B **79**, 054504 (2009); W. Lv, J. Wu, and P. Phillips, *ibid.* **80**, 224506 (2009); C.-C. Chen, B. Moritz, J. van den Brink, T. P. Devereaux, and R. R. P. Singh, *ibid.* **80**, 180418 (2009).

[27] J.-H. Chu, J. G. Analytis, K. D. Greve, P. L. McMahon, Z. Islam, Y. Yamamoto, and I. R. Fisher, Science **329**, 824 (2010); J. J. Ying, X. F. Wang, T. Wu, Z. J. Xiang, R. H. Liu, Y. J. Yan, A. F. Wang, M. Zhang, G. J. Ye, P. Cheng, J. P. Hu, and X. H. Chen, e-print arXiv:1012.2731.

[28] E. C. Blomberg, M. A. Tanatar, A. Kreyssig, N. Ni, A. Thaler, R. Hu, S. L. Bud'ko, P. C. Canfield, A. I. Goldman, and R. Prozorov, Phys. Rev. B **83**, 134505 (2011).

[29] A. Dusza, A. Lucarelli, F. Pfuner, J.-H. Chu, I. R. Fisher, and L. Degiorgi, e-print arXiv:1007.2543; M. Nakajima *et al.* (unpublished).

[30] R. M. Fernandes, L. H. VanBebber, S. Bhattacharya, P. Chandra, V. Keppens, D. Mandrus, M. A. McGuire, B. C. Sales, A. S. Sefat, and J. Schmalian, Phys. Rev. Lett. **105**, 157003 (2010).

[31] M. Yoshizawa, R. Kamiya, R. Onodera, Y. Nakanishi, K. Kihou, H. Eisaki, and C. H. Lee, e-print arXiv:1008.1479.

[32] M. Yoshizawa *et al.* (private communication).

[33] T. Goto, R. Kurihara, K. Araki, K. Mitsumoto, M. Akatsu, Y. Nemoto, S. Tatematsu, and M. Sato, J. Phys. Soc. Jpn. **80**, 073702 (2011); T. Goto *et al.* (unpublised).

[34]J. Zhao, D. T. Adroja, D.-X. Yao, R. Bewley, S. Li, X. F. Wang, G. Wu, X. H. Chen, J. Hu, and P. Dai, Nat. Phys. **5**, 555 (2009).
[35]W. A. Little, Phys. Rev. **134**, A1416 (1964).
[36]V. L. Ginzburg, Zh. Eksp. Teor. Fiz. **47**, 2318 (1964) [Sov. Phys. JETP **20**, 1549 (1965)].
[37]J. E. Hirsch and D. J. Scalapino, Phys. Rev. Lett. **56**, 2732 (1986).
[38]V. Cvetkovic and Z. Tesanovic, Europhys. Lett. **85**, 37002 (2009).
[39]M. Berciu, I. Elfimov, and G. A. Sawatzky, e-print arXiv:0811.0214.
[40]T. Takimoto, T. Hotta, T. Maehira, and K. Ueda, J. Phys. Condens. Matter **14**, L369 (2002).
[41]Y. Yanagi, Y. Yamakawa, and Y. Ono, Phys. Rev. B **81**, 054518 (2010).
[42]T. Miyake, K. Nakamura, R. Arita, and M. Imada, J. Phys. Soc. Jpn. **79**, 044705 (2010).
[43]Y. Yanagi, Y. Yamakawa, N. Adachi, and Y. Ono, J. Phys. Soc. Jpn. **79**, 123707 (2010).
[44]H. Kontani and S. Onari, J. Phys. Soc. Jpn. **80**, 056001 (2011).
[45]J. R. Schrieffer, *Theory of Superconductivity* (Benjamin, New York, 1964).
[46]In Ref. 43, $\chi^{Q}_{x^2-y^2}(\boldsymbol{q},0)$ due to the "orthorhombic phonon" ($=g_{66}$ in the present paper) is incommensurate with momentum $\boldsymbol{q} \approx (0.35\pi,0)$. In the present tight-binding model,[2] $\chi^{Q}_{x^2-y^2}(\boldsymbol{q},0)$ due to g_{66} has the highest peak at $\boldsymbol{q} \approx (\pi,0)$ due to the nesting between electron and hole pockets, while it is hardly enhanced at $\boldsymbol{q} = \boldsymbol{0}$.
[47]K. Yada and H. Kontani, Phys. Rev. B **77**, 184521 (2008); J. Phys. Soc. Jpn. **75**, 033705 (2006).
[48]In Ref. 10, we claimed that the enhancement of $\chi^{Q}_{xz}(\boldsymbol{0},0)$ in the five-orbital model induces the softening of C_{44}. However, it was incorrect since the effect of unfold-gauge transformation on $\chi^{Q}_{xz}(\boldsymbol{0},0)$ was overlooked. In fact, $\chi^{Q}_{xz}(\boldsymbol{0},0)$ is not enhanced in the ten-orbital model.
[49]H. Kontani and K. Yamada, J. Phys. Soc. Jpn. **65**, 172 (1996).
[50]L. Boeri, O. V. Dolgov, and A. A. Golubov, Phys. Rev. Lett. **101**, 026403 (2008).
[51]P. Thalmeier and B. Luthi, in *Handbook on the Physics and Chemistry of Rare Earths*, edited by K. A. Gschneidner Jr. and L. Eyring (Elsevier, Amsterdam, 1991), Vol. 14, p. 245.
[52]P. M. Levy, P. Morin, and D. Schmitt, Phys. Rev. Lett. **42**, 1417 (1979).
[53]L. G. Aslamasov and A. I. Larkin, Sov. Phys. Solid State **10**, 875 (1968).
[54]H. Fukuyama, H. Ebisawa, and T. Tsuzuki, Prog. Theor. Phys. **46**, 1028 (1971).
[55]I. Ussishkin, Phys. Rev. B **68**, 024517 (2003).
[56]T. Moriya, *Spin Fluctuations in Itinerant Electron Magnetism* (Springer-Verlag, Berlin, 1985); T. Moriya and K. Ueda, Adv. Phys. **49**, 555 (2000); Rep. Prog. Phys. **66**, 1299 (2003).
[57]A. A. Abricosov, L. P. Gor'kov, and I. E. Dzyaloshinskii, *Methods of Quantum Field Theory in Statistical Physics* (Dover, New York, 1975).
[58]H. Shishido, A. F. Bangura, A. I. Coldea, S. Tonegawa, K. Hashimoto, S. Kasahara, P. M. C. Rourke, H. Ikeda, T. Terashima, R. Settai, Y. Onuki, D. Vignolles, C. Proust, B. Vignolle, A. McCollam, Y. Matsuda, T. Shibauchi, and A. Carrington, Phys. Rev. Lett. **104**, 057008 (2010).
[59]K. Kubo and P. Thalmeier, J. Phys. Soc. Jpn. **78**, 083704 (2009); C.-C. Lee, W.-G. Yin, and W. Ku, Phys. Rev. Lett. **103**, 267001 (2009); H. Oh, D. Shin, and H. J. Choi, e-print arXiv:1012.2224.
[60]K. Sugimoto, E. Kaneshita, and T. Tohyama, J. Phys. Soc. Jpn. **80**, 033706 (2011).
[61]H. Kontani (unpublished).
[62]C.-C. Chen, J. Maciejko, A. P. Sorini, B. Moritz, R. R. P. Singh, and T. P. Devereaux, Phys. Rev. B **82**, 100504(R) (2010).